NANOSOLDERING CARBON NANOTUBE FIBERS AND GRAPHENE NANORIBBON THIN FILM TRANSISTORS

BY

SIDDHANTH MUNUKUTLA

THESIS

Submitted in partial fulfillment of the requirements
for the degree of Master of Science in Electrical and Computer Engineering
in the Graduate College of the
University of Illinois at Urbana-Champaign, 2017

Urbana, Illinois

Adviser:

Professor Joseph W. Lyding

Abstract

In this thesis, we explore the electronics applications of the nanoscale allotropes of carbon. We work with carbon nanotubes and graphene nanoribbons. The first part involves using carbon nanotubes (CNTs) to build composite structures such as fibers. In the past, our group developed the “nanosoldering” technique to solder carbon nanotube junctions which significantly improved the electrical properties of CNT transistors. For the purpose of our work, we apply the nanosoldering technique to the CNT junctions in the fibers to enhance their properties. We study the electrical and thermal properties of the fibers before and after nanosoldering. We measure the electrical conductivity using a four-terminal sensing circuit, and an IR microscope is used to map the real-time temperature profile of the fibers to extract thermal conductivity.

In the second part, we also fabricate and characterize transistors from thin films of atomically precise graphene nanoribbons (GNRs). Device studies of solution synthesized GNRs have been limited because of poor processing. In this work, a novel interfacial self-assembly approach is used to produce uniform thin films of GNRs. Transistors are then fabricated using the GNR thin films as the channel material and the resulting devices are characterized.

To my family, for their unconditional love and support.

Acknowledgments

I would like to thank my advisor Prof. Joseph Lyding for his tremendous support and encouragement throughout my undergraduate and graduate education. Prof. Lyding has always been patient, and helpful. He has been supportive of my ideas and taught me to think very critically when searching for answers. It has been a privilege to be in his research group and to work at the forefront of nanotechnology.

My development into a graduate researcher would not have also been possible without the early support of Adrian Radocea. Adrian's guidance during my undergraduate days taught me to be a more responsible student and researcher and this has helped me a lot in graduate school. I want to thank Dr. Jae Won Do for his guidance and advice on device fabrication which aided the graphene nanoribbon thin film transistor project. The fabrication and characterization of the carbon nanotube fibers would not have been possible without the tremendous support and contribution of Dr. Gang Wang. I would like to thank him for his part in making chapter 2 possible. I would like to thank the rest of the Lyding Group for being supportive and helpful throughout my research, including Dr. Pamela Martin, Dr. Yingjie Zhang, Duc Nguyen, Faraz Arastu, Huy Nguyen, Kaitlyn Parsons, Sartaj Grewal, Ximeng Liu, and Yaofeng Chen.

I want to thank and acknowledge the contributions of our collaborators. The 1,3,5-tris(2-bromophenyl)benzene (2-TBB) molecule used for the nanosoldering process in chapter 2 was synthesized by Prof. Greg Girolami's graduate student Peter Sempsrott in the Chemistry Department. Prof. Eric Pop and his graduate student Feifei Lian of Stanford University performed the thermal conductivity measurements of the carbon nanotube fibers. The work presented in chapter 2 was supported by the National Science Foundation's Power Optimization of Electro-Thermal Systems (POETS) engineering research center. I am thankful for the funds provided by

POETS and the collaborations that it allowed which contributed to this thesis. The graphene nanoribbons used in chapter 3 were synthesized by Prof. Alexander Sinitskii's graduate student Timothy Vo of the University of Nebraska-Lincoln (UNL). I want to thank and acknowledge UNL students Mikhail Shekhirev, Mohammad Mehdi Pour, and Alexey Lipatov for the fabrication and characterization of the graphene nanoribbon thin films that made the graphene nanoribbon thin film transistor project possible. The work presented in thesis was performed at the Beckman Institute for Advanced Science and Technology, the Micro and Nanotechnology Lab (MNTL) and the Frederick Seitz Materials Research Laboratory (MRL). I would like to thank the kind and courteous staff at these research labs for training me on the tools and equipment that contributed to my experiments.

I am more than grateful to the ECE department at UIUC. I would not be the engineer that I am today without its rigorous and fulfilling education. I would like to thank Profs. Jean-Pierre Leburton, John Dallesasse and Xiuling Li. Their courses in semiconductor device physics and fabrication have continued to stimulate my interest in this field and helped me with my research. The ECE department has also provided me with various scholarships, fellowships and awards over the years, and this has helped finance my education and other living expenses. I want to acknowledge the various student organizations that I have been a part of over the years including the ECE Student Advancement Committee (ECESAC), Eta Kappa Nu (HKN) Alpha Chapter and Promoting Undergraduate Research in Engineering (PURE). These organizations provided me with a sense of fulfillment outside of my academics and they taught me the importance and value of good leadership and teamwork.

My six years here were amazing because of my friends who provided fun and support, and helped me evolve into a better person. I am indebted to all of them and I hope we continue to stay

in touch wherever we go. Finally, I would like to thank my family and especially my parents and my brother. They have always encouraged me to push myself further and I could not have come this far without their unconditional love and support. I dedicate this thesis to them.

Table of Contents

1. Introduction

1.1 Carbon Based Materials

Silicon is the second most abundant element in the earth's crust. This can be seen in figure 1, which shows the abundance of each element with respect to the atomic number. Silicon's abundance makes it the backbone of modern electronics. Another element that is of interest to us is carbon. Carbon is the 15th most abundant element in the earth's crust and this also makes it a good candidate for electronic applications.

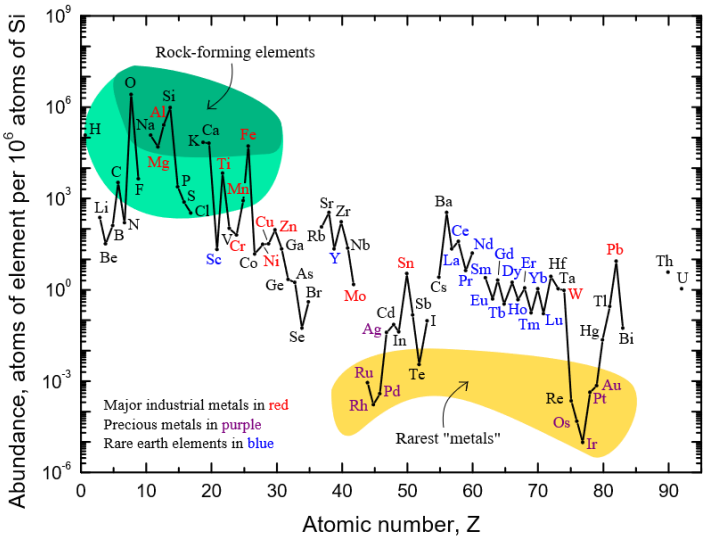

Figure 1: Abundance of the elements in the Earth's crust as a function of atomic number. [1]

As a result of its valency, carbon is capable of existing in many different physical forms (allotropes). The most well-known and naturally occurring allotropes are diamond and graphite. These allotropes are vastly different from each other and their structures tell us that the alignment of carbon atoms have profound effects on the material properties.

Over the past three decades, nanoscale sized allotropes of carbon have emerged and their discovery has created avenues for new technologies. Spherical fullerene or buckminsterfullerene

(C_{60}) was discovered in 1985 [2] and carbon nanotubes (CNTs) were discovered in 1991 [3]. In 2004, the Manchester group isolated a single layer of carbon atoms (graphene) from graphite [4]. These nanoscale allotropes can be categorized by dimensionality and the schematics of each material are shown in figure 2.

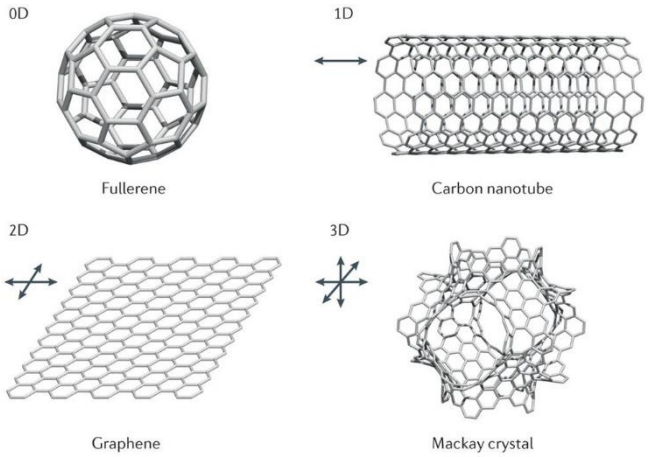

Figure 2: Structural representations of nanoscale allotropes of carbon organized by their dimensionality. [5]

The nanoscale allotropes of carbon can conduct electricity, absorb and emit light, and exhibit magnetic properties. Their attractive properties give them potential applications in materials science, synthetic biology and electronics. While fullerenes and Mackay crystals are appealing, in this thesis we focus on carbon nanotube and graphene nanoribbons (GNRs). Our interest is particularly in the electronics applications of these materials, and in the following sections we offer a brief introduction to CNTs and GNRs.

1.2 Carbon Nanotubes

Carbon nanotubes (CNTs) were discovered by Sumio Iijima in 1991 while working at NEC Corporation in Japan [3]. Iijima's discovery generated a significant interest in carbon based nanostructures which fueled research in nanotechnology. CNTs can be considered as one-dimensional cylinders [6] of monolayer graphene. A further classification splits CNTs into single-walled (SW) and multi-walled (MW) nanotubes. A multi-walled nanotube contains several concentric tubes. In a random network of CNTs, approximately two-thirds of the CNTs possess semiconducting properties and one-third possess metallic properties [7]. This is illustrated in figure 3.

Figure 3: A schematic illustration of a graphene sheet being rolled up into a CNT. Depending on how the sheet is rolled up, the resulting CNT can be either semiconducting or metallic. [7]

CNTs have been researched extensively for numerous applications because of their superb electrical [8-10], thermal [11-13], chemical [14, 15], and mechanical [16, 17] properties. In this thesis, we explore the use of carbon nanotubes in fibers (composite structures) and aim to tackle some of the problems presented in these composite structures.

1.3 Graphene and Graphene Nanoribbons

As previously mentioned, graphene was first isolated in 2004 by the Manchester group using Scotch tape based micromechanical exfoliation [3]. For their groundbreaking work, Andre Geim and Konstantin Novoselov received the Nobel Physics prize in 2010. This new material quickly attracted the attention of the electron device community and today major semiconductor companies are active in graphene research. The International Technology Roadmap for Semiconductors (ITRS), the strategic planning document for the semiconductor industry, considers graphene to be a candidate for post-silicon electronics [18].

The greatest advantage of graphene is its high carrier mobility at room temperature. Mobilities of 10,000 – 15,000 $cm^2V^{-1}s^{-1}$ [4, 19] have been measured for graphene on silicon wafers and an upper limit between 40,000 and 70,000 $cm^2V^{-1}s^{-1}$ [19, 20] has been suggested. While these numbers are impressive and make graphene a compelling candidate, large area graphene is a semi-metal with a zero bandgap. Its valence and conduction bands are cone-shaped and meet at the K points of the Brillouin zone. This can be seen in the red graph of figure 4. Since graphene has a zero bandgap, devices using graphene as a channel material cannot be switched off and are thus unsuitable for logic applications.

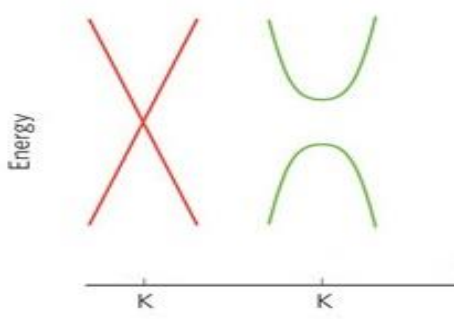

Figure 4: Band structure around the K-point of graphene (red) and graphene nanoribbons (green). [21]

A bandgap can be opened in graphene by confining it to a narrow strip. This can be explained by the principle of quantum confinement. When graphene is isolated into a narrow "ribbon" the carriers are confined to a quasi-one-dimensional system; this opens an energy gap [22] and the bands become parabolic as shown in the green graph of figure 4. The narrowed graphene material is called a graphene nanoribbon (GNR) and it can be used in electronics devices.

Theoretical predictions have shown that armchair nanoribbons and zigzag nanoribbons have a bandgap that is inversely proportional to the width of the nanoribbon [23]. A schematic of an armchair nanoribbon is shown in figure 5. In order to use a graphene nanoribbon for conventional FETs, well-defined (atomically precise) edges are required.

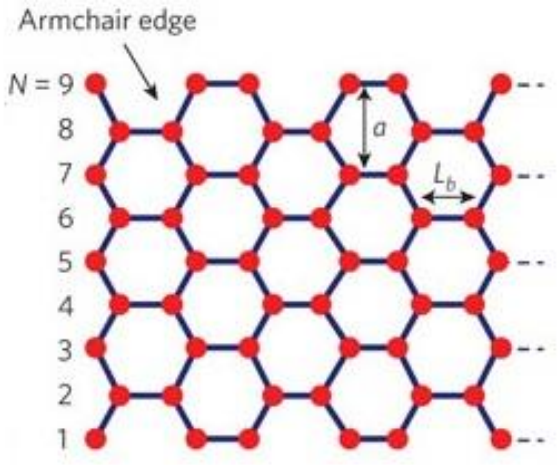

Figure 5: Schematic of an armchair graphene nanoribbon. [21]

In this thesis, we explore the use of thin films from atomically precise graphene nanoribbons in FET devices. We fabricate and characterize the resulting devices.

1.4 Thesis Structure

The purpose of this thesis is to explore the applications of carbon based nanomaterials in electronics. Chapter 2 focuses on CNT fibers and chapter 3 focuses on transistors from thin films of atomically precise graphene nanoribbons (GNRs).

In chapter 2, we focus on CNT fibers and attempt to improve their electronic and thermal properties by applying the "nanosoldering" technique that our research group developed to solve the problems caused by CNT junctions. This chapter presents a fabrication procedure for the CNT fibers and data from scanning electron microscopy (SEM), Raman spectroscopy, and thermal infrared (IR) imaging. Current-voltage curves will also be shown to highlight the electrical properties of the fibers and the improvement observed from nanosoldering.

In chapter 3, we focus on transistors from thin films of atomically precise graphene nanoribbons (GNRs). This chapter highlights the synthesis of the GNRs, and the subsequent transistor fabrication. Data from SEM and Raman spectroscopy will be presented. Current-voltage curves will also be presented to highlight transistor performance. It should be noted that the work presented in chapter 3 was published in the journal *ACS Applied Materials & Interfaces* [24].

Finally, chapter 4 summarizes and discusses the results of the work presented in chapters 2 and 3. It will conclude with an outlook for future work and other exciting avenues.

1.5 References

[1] M. Diggles, "Rare earth Elements—Critical resources for high technology," in *U.S. Geological Survey Fact Sheet 087-02*, 2002. [Online]. Available: https://pubs.usgs.gov/fs/2002/fs087-02/. Accessed: Feb. 27, 2017.

[2] H. W. Kroto, J. R. Heath, S. C. O'Brien, R. F. Curl, and R. E. Smalley, "C60: Buckminsterfullerene," *Nature*, vol. 318, no. 6042, pp. 162–163, Nov. 1985.

[3] S. Iijima, "Helical microtubules of graphitic carbon," *Nature*, vol. 354, no. 6348, pp. 56–58, Nov. 1991.

[4] K. S. Novoselov et al., "Electrical field effect in atomically thin carbon films," *Science*, vol. 306, no. 5696, pp. 666–669, Oct. 2004.

[5] S. Yasumoto, H. Ito, and K. Itami, "Structurally uniform and atomically precise carbon nanostructures," *Nature Reviews Materials*, vol. 1, no. 1, pp. 15002, Jan. 2016.

[6] R. Saito, M. Fujita, G. Dresselhaus, and M. S. Dresselhaus, "Electronic structure of chiral graphene tubules," *Applied Physics Letters*, vol. 60, no. 18, pp. 2204–2206, Mar. 1992.

[7] P. G. Collins and P. Avouris, "Nanotubes for electronics," Scientific American, vol. 283, pp. 62–69, Dec. 2000.

[8] Q. Cao, S.-J. Han, G. S. Tulevski, Y. Zhu, D. D. Lu, and W. Haensch, "Arrays of single-walled carbon nanotubes with full surface coverage for high-performance electronics," *Nature Nanotechnology*, vol. 8, no. 3, pp. 180–186, Jan. 2013.

[9] J. Appenzeller, "Carbon nanotubes for high-performance electronics– Progress and prospect," *Proc. IEEE*, vol. 96, no. 2, pp. 201–211, Jan. 2008.

[10] S. J. Tans, A. R. M. Verschueren, and C. Dekker, "Room-temperature transistor based on a single carbon nanotube" *Nature*, vol. 393, no. 6680, pp. 49–52, May 1998.

[11] A. Behnam et al., "High-field transport and thermal reliability of sorted carbon nanotube network devices," *ACS Nano*, vol. 7, no. 1, pp. 482–490, Dec. 2012.

[12] M. A. Panzer et al., "Thermal properties of metal-coated vertically aligned single-wall nanotube arrays," *Journal of Heat Transfer*, vol. 130, no. 5, p. 52401, May 2008.

[13] Z. Han and A. Fina, "Thermal conductivity of carbon nanotubes and their polymer nanocomposites: A review," *Progress in Polymer Science*, vol. 36, no. 7, pp. 914–944, Jul. 2011.

[14] P. Bondavalli, P. Legagneux, and D. Pribat, "Carbon nanotubes based transistors as gas sensors: State of the art and critical review," *Sensors and Actuators B: Chemical*, vol. 140, no. 1, pp. 304–318, May 2009.

[15] K. Maehashi and K. Matsumoto, "Label-free electrical detection using carbon nanotube-based biosensors," *Sensors*, vol. 9, no. 7, pp. 5368–5378, Jul. 2009.

[16] R. Zhang, Q. Wen, W. Qian, D. S. Su, Q. Zhang, and F. Wei, "Superstrong ultralong carbon nanotubes for mechanical energy storage," *Advanced Materials*, vol. 23, no. 30, pp. 3387–3391, Jun. 2011.

[17] J. Di et al., "Ultrastrong, foldable, and highly conductive carbon nanotube film," *ACS Nano*, vol. 6, no. 6, pp. 5457–5464, May 2012.

[18] "ITRS Reports," in *International Technology Roadmap for Semiconductors*, International Technology Roadmap for Semiconductors. [Online]. Available: http://www.itrs2.net/itrs-reports.html. Accessed: Feb. 27, 2017.

[19] J.-H. Chen, C. Jang, S. Xiao, M. Ishigami, and M. S. Fuhrer, "Intrinsic and extrinsic performance limits of graphene devices on SiO_2," *Nature Nanotechnology*, vol. 3, no. 4, pp. 206–209, Mar. 2008.

[20] F. Chen, J. Xia, D. K. Ferry, and N. Tao, "Dielectric screening enhanced performance in graphene FET," *Nano Letters*, vol. 9, no. 7, pp. 2571–2574, Jun. 2009.

[21] F. Schwierz, "Graphene transistors," *Nature Nanotechnology*, vol. 5, no. 7, pp. 487–496, May 2010.

[22] M. Y. Han, B. Özyilmaz, Y. Zhang, and P. Kim, "Energy band-gap engineering of graphene nanoribbons," *Physical Review Letters*, vol. 98, no. 20, p. 206805, May 2007.

[23] L. Yang, C.-H. Park, Y.-W. Son, M. L. Cohen, and S. G. Louie, "Quasiparticle energies and band gaps in graphene nanoribbons," *Physical Review Letters*, vol. 99, no. 18, p. 186801, Nov. 2007.

[24] M. Shekhirev et al., "Interfacial self-assembly of atomically precise graphene nanoribbons into uniform thin films for electronics applications," *ACS Applied Materials & Interfaces*, vol. 9, no. 1, pp. 693–700, Dec. 2016.

2. Nanosoldering Carbon Nanotube Fibers

2.1 Nanosoldering as a Mechanism for Self-Healing

As previously mentioned, CNTs are explored extensively because of their outstanding electrical, thermal, and mechanical properties. While CNT networks are relatively easy to fabricate and exhibit promise, the performance of these networks is limited by CNT-CNT inter-tube junctions (CNT junctions). Carrier mobility, conductivity and power dissipation are greatly limited by the resistance at the CNT junctions. Theoretical and experimental studies have revealed that the electrical [1-6] and thermal resistances [7-11] at these junctions are at least an order of magnitude higher than those of individual CNTs. Thus, passing current through a CNT network causes localized heating at these CNT junctions which lowers a device's performance and reliability.

To combat this problem, efforts have been made to lower the CNT junction resistance by depositing nanoscale metallic particles at the CNT junctions. Previous studies have utilized AFM assisted dip pen nanolithography [12] and transmission electron microscopy (TEM) facilitated electron beam induced deposition [13]. While these techniques are unique and elegant, they need slow and repetitive processes that need to locate individual junctions.

Our research group developed the "nanosoldering" technique to selectively deposit metal particles at the CNT junctions using a gas phase CVD process [14] and a solution based approach [15]. The nanosoldering process lowers the resistivity of the CNT junctions in the CNT networks by cooling them. In the gas phase CVD process, devices are loaded into a vacuum chamber and a CVD precursor, either $C_5H_5PdC_3H_5$ or $Hf(BH_4)_4$, is introduced into the chamber. When current is passed through the devices, the resistance at the CNT junctions generates "hot spots" which cause a local chemical reaction depositing either Pd or HfB_2 at the CNT junctions. The process improved the I_{on}/I_{off} ratio by an order of magnitude. Figure 6 depicts the nanosoldering procedure and the

inset displays an $I_{DS} - V_{GS}$ curve of a CNT transistor, before and after nanosoldering. Figure 7 (a) shows SEM images of CNT transistors before and after nanosoldering. The deposited HfB_2 can be seen in yellow and energy dispersive x-ray spectroscopy (EDS) is used to verify the presence of the HfB_2 at the CNT junctions. This can be seen in figure 7 (b).

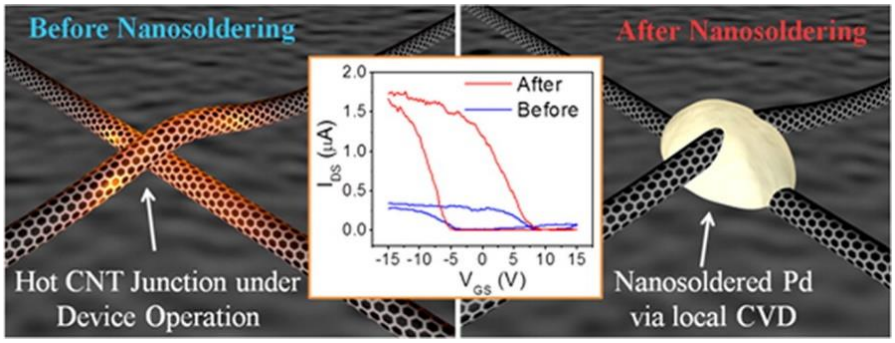

Figure 6: An illustration of the nanosoldering process. The inset shows an I-V curve of a CNT device before and after nanosoldering. An order of magnitude in improvement in the on/off ratio is observed. [14]

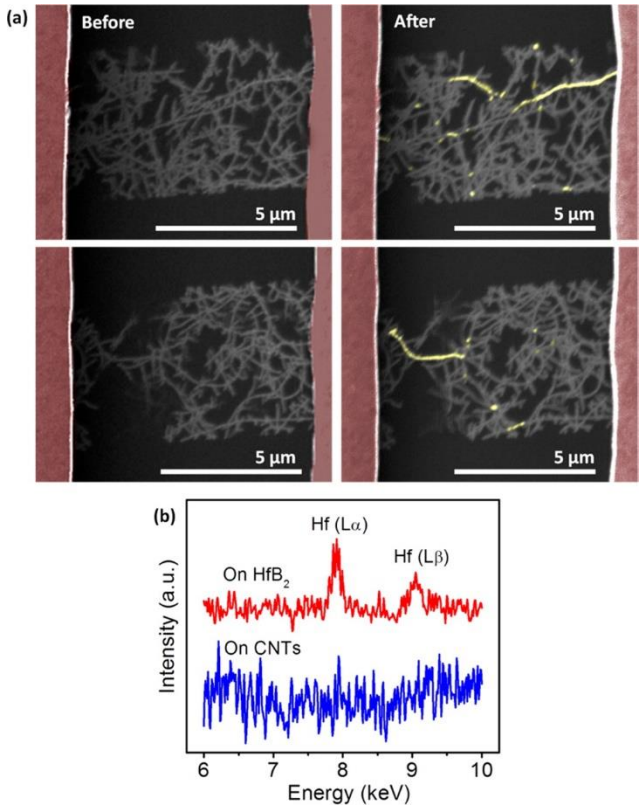

Figure 7: (a) An SEM image of a CNT device before (left) and after (right) nanosoldering. The HfB_2 is false colored in yellow. (b) EDS spectra from HfB_2 deposited at the nanotube junctions (red) and on CNTs from the same device when no HfB_2 was deposited (blue). [14]

The solution based approach also accomplishes this and it is a simpler alternative to the CVD method. In this approach, $Pd_2(dba)_3$ is mixed in a volatile solvent and the solution is spin-coated onto a device forming a thin film of the precursor on top of the CNT networks. Passing current through the devices causes localized heating at the CNT junctions and generates thermal decomposition of the precursor. Once the Pd nanoparticles are deposited at the junctions, the solution and all byproducts of the thermal decomposition reaction are rinsed away. This process improved the I_{on}/I_{off} ratio and mobility of the CNT networks by an average factor of ~6. The solution based process is highlighted in figure 8 and $I_{DS} - V_{GS}$ curves of transistors, before and after nanosoldering, are shown in figure 9. Figure 10 displays an SEM image of a CNT network with the deposited Pd nanoparticles.

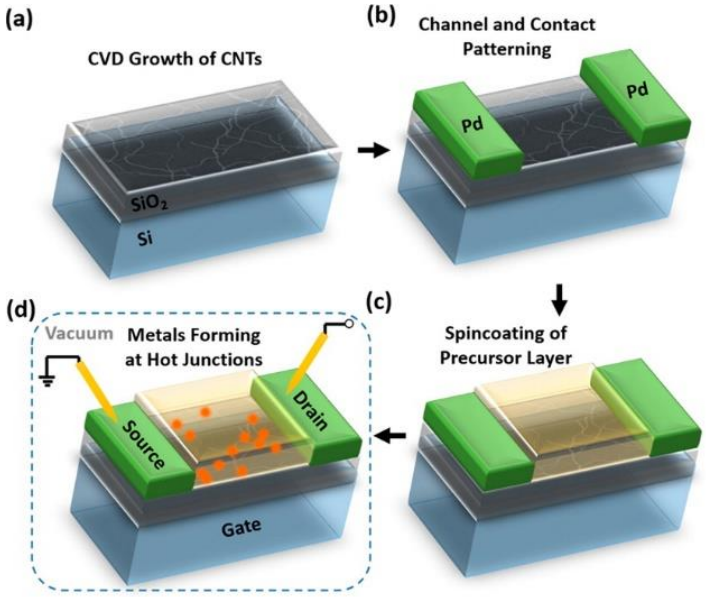

Figure 8: Schematic diagrams of (a) carbon nanotube (CNT) network growth on a SiO_2/Si substrate by chemical vapor deposition (CVD). (b) Devices were fabricated using photolithography and e-beam evaporation for channel and contact patterning with Ti/Pd (0.5/40 nm) electrodes. (c) Solution-mediated application of the $Pd_2(dba)_3$ precursor onto CNT networks by spin-coating. (d) Selective Pd deposition triggered by resistive heating at CNT junctions under device operation in a vacuum probe station. [15]

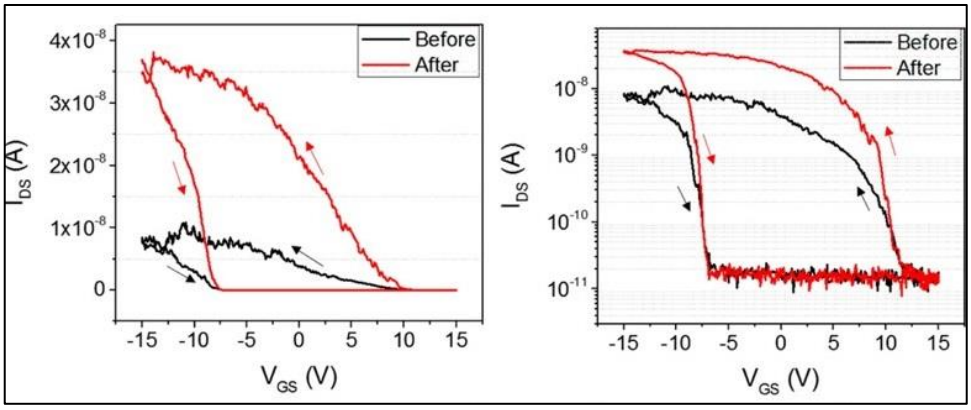

Figure 9: I-V curve of a CNT device before and after nanosoldering in linear (left) and log (right) scales. The on/off ratio improved by a factor of ~4.4. [15]

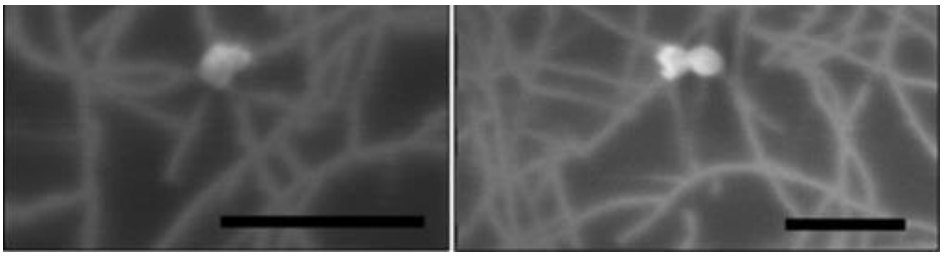

Figure 10: Magnified SEM images of a CNT network showing CNT junctions nanosoldered with Pd particles. The scale bar is 1μm. [15]

2.2 Nanosoldering with Organic Molecules

In the previous section, we described an approach demonstrated by our research group that selectively deposits metal nanoparticles at CNT junctions utilizing a local chemical reaction. Instead of using metal nanoparticles, we believe that by using carbon atoms to link the CNT junctions, the results of the nanosoldering process could be further amplified. The covalent network of carbon atoms can lead to further improvement in electrical performance by creating an all-carbon system with work function matching at the CNT junctions.

The molecule 1,3,5-tris(2-bromophenyl)benzene (2-TBB) is used as the precursor and it is dissolved into chloroform and spin-coated onto the CNT devices. Passing current through the devices heats the CNT junctions which causes a chemical reaction. The chemical reaction should

result in a debrominated and dehydrogenated all-carbon structure resembling graphene nanoribbons.

The 2-TBB molecules used in this section and in the remainder of this chapter were synthesized by Dr. Peter Sempsrott, a former graduate student in Professor Girolami's group in the Chemistry Department at UIUC. The synthesis is described in Dr. Jae Won Do's PhD thesis [16]. 2-bromoacetophene (2.7 mL, 20.0 mmol) was added (via syringe) to a small oven-dried Schlenk tube under argon. Trifluoromethanesulfonic acid (TfOH) (0.2 mL, 2.3 mmol) was also added (via syringe) and the solution was heated under active argon flow to 130 °C for 7 hours with stirring. The resulting dark brown solution was cooled to room temperature, quenched with ~20 mL of water and extracted with dichloromethane. The organic layer was dried with $MgSO_4$ and evaporated. The crude residue was purified by silica gel chromatography eluting with pentane/dichloromethane (6:1) to give a light yellow solid. The solid was recrystallized from hexane/dichloromethane to afford 1.336 g (37% yield) of white crystalline powder. The 2-TBB powder can be seen in figure 11, and figure 12 shows the synthesis procedure. Figure 13 depicts the process for producing the all-carbon structure from the 2-TBB.

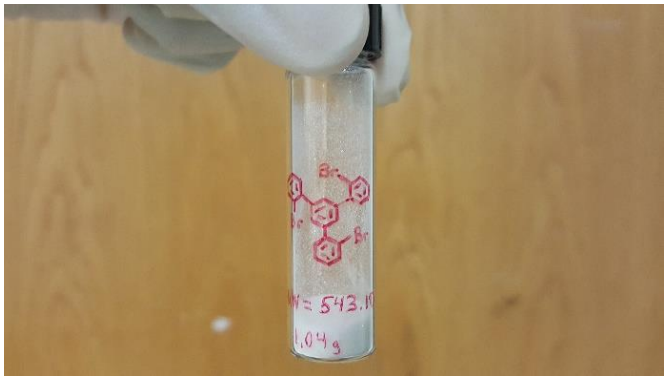

Figure 11: 2-TBB powder used for the organic nanosoldering process.

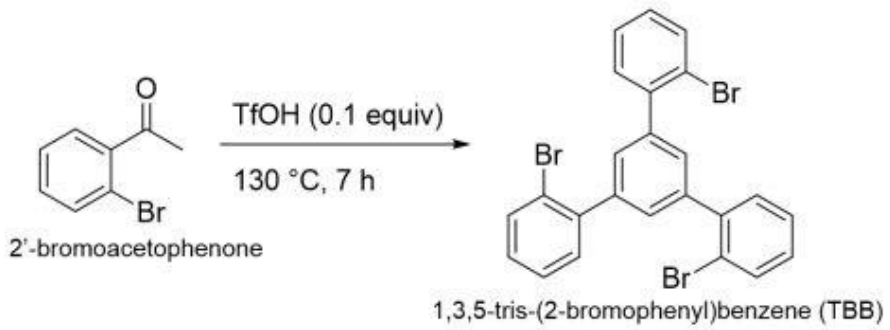

Figure 12: Synthesis scheme for 1,3,5-tris(2-bromophenyl)benzene (2-TBB) from 2'- bromoacetophenone. [16]

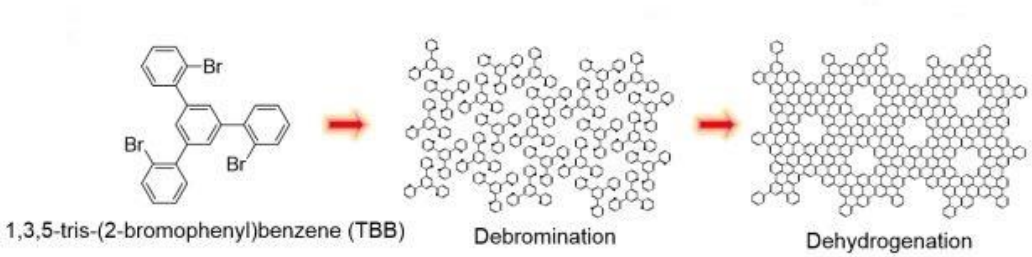

Figure 13: Process for producing the all-carbon structure from the 2-TBB. [16]

As mentioned previously, 60 – 80 mg of 2-TBB is dissolved in 2 – 3 mL of chloroform and spin-coated onto the CNT transistor devices. The devices were loaded into a Janis Variable Temperature Probe Station with a pressure of ~10^{-5} Torr. After that, V_{DS} was applied from 1 V and increased in 5 V increments up to 130 V while V_{GS} was swept from -20 V to +20 V. The preliminary results of this approach were very promising, but unlike the nanosoldering process with the Pd/HfB_2 particles we cannot see anything at the CNT junctions with SEM imaging. This is because the all-carbon structure that covalently links the junctions is too small to be seen. I_{DS} – V_{GS} curves of transistors, before and after the nanosoldering process, are shown in figure 14.

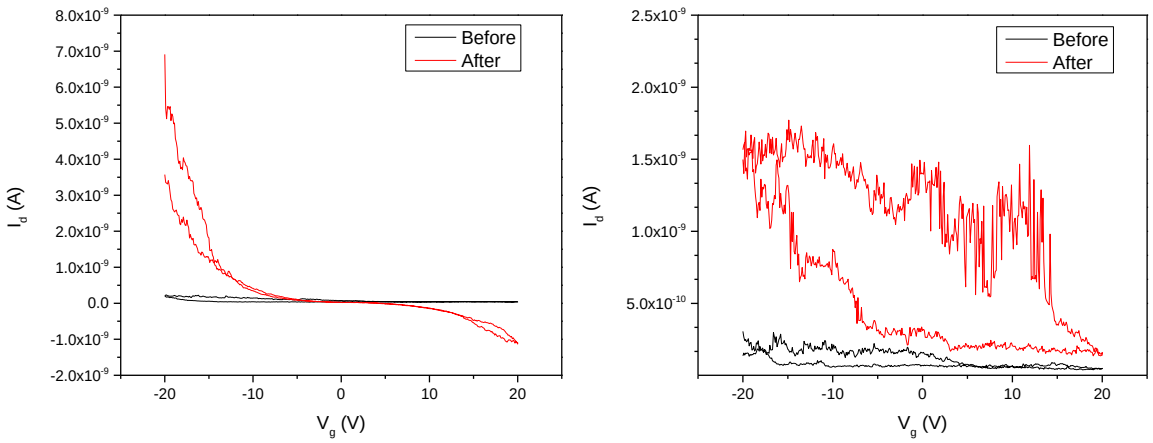

Figure 14: I-V Characteristics of CNT transistors using organic molecules for the nanosoldering process.

The preliminary results of the organic nanosoldering process with CNT transistors show that our technique can be extended to organic molecules as well. In the following sections we apply the organic nanosoldering procedure to CNT fibers. The purpose of this is to improve the electrical and thermal conductivity of the CNT fibers by lowering the resistance and cooling the CNT junctions in these CNT composite structures.

2.3 Carbon Nanotube Fibers

Conventional electric wires comprised of copper and aluminum suffer from weight issues, the skin effect, mechanical performance and electromigration [17]. These metal conductors are required and their increasing prices suggest the need for a low-cost material that can outperform conventional metal conductors. Fibers have had a significant impact on aerospace, military and industrial applications requiring lightweight, mechanically strong materials [18].

The excellent properties of CNTs make them compelling candidates for fiber applications. Fibers comprised of CNTs have the potential to form high-strength, lightweight, thermally and electrically conducting materials [19].

CNT fibers can be produced through either wet or dry spinning [20]. Wet spinning techniques rely on the extrusion of a liquid solution of CNTs into a bath with a liquid which can mix with the solvent, but cannot disperse the nanotubes [20]. This technique begins with a liquid and is converted into the form of fibers by alignment.

Dry spinning methods are either a one-step or two-step process. In the one-step process, fibers are drawn directly from a CVD reactor [21-24], and in the two-step process, fibers are spun from other CNT assemblies such as CNT arrays [25, 26, 27], CNT cotton [28, 29] and CNT films [30, 31]. An example of a wet-spinning method where CNT fibers are spun from liquid crystalline phase is shown in figure 15, and a dry spinning method where CNT fibers are drawn from a CNT array is shown in figure 16.

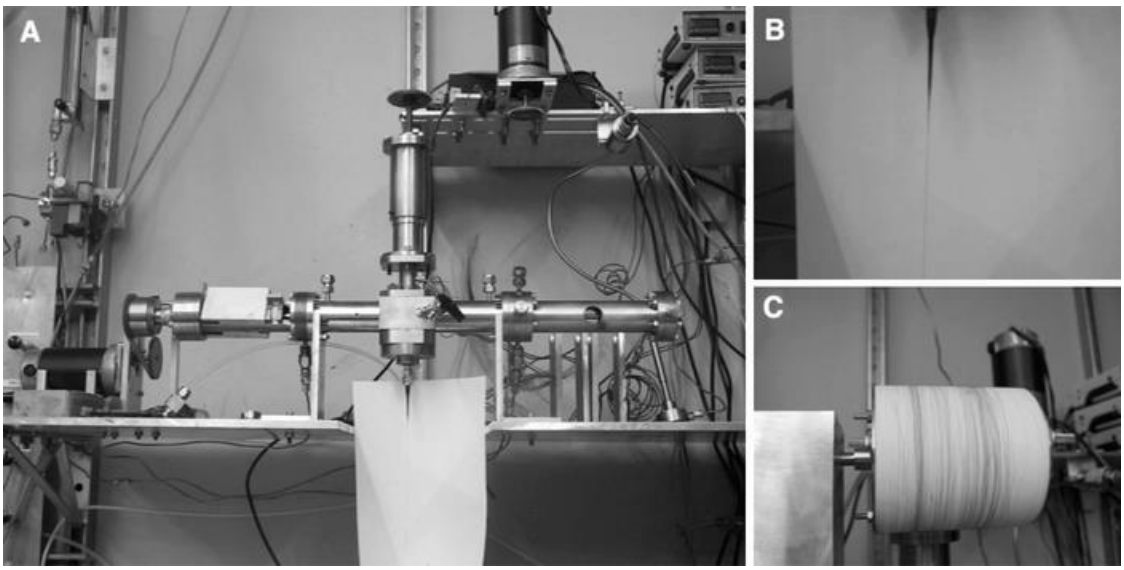

Figure 15: (A) The system used by Ericson et al. to spin CNT fibers from liquid crystalline phase. (B) Fiber extruded from a capillary tube. (C) CNT fiber wound on a rotating spool. [39]

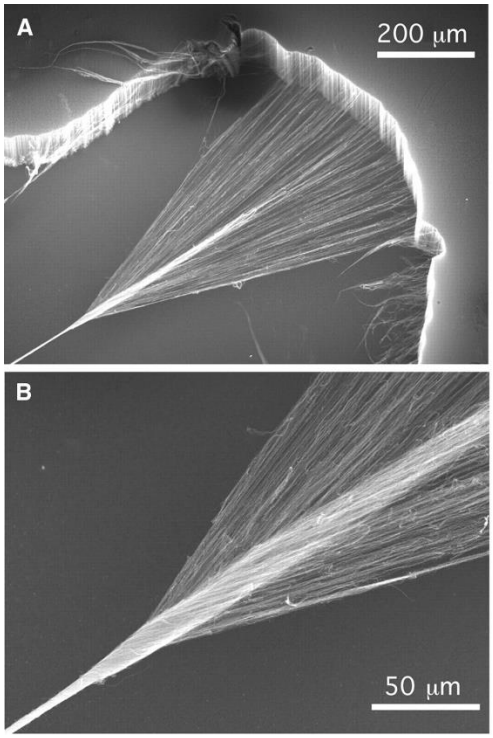

Figure 16: (A) SEM image of a CNT fiber spun from a CNT yarn. (B) A magnified SEM image of (A) showing the individual fibers. [25]

For the purpose of this thesis, we use the fabrication method presented by Vigolo et al. [32]. In this method, CNTs are dispersed in surfactant solutions and then coagulated into a fiber by streaming them in the presence of a polymer solution. A schematic of the experimental setup is shown in figure 17. It must be noted that our experimental setup does not use a rotating stage and this will be shown in section 2.4.

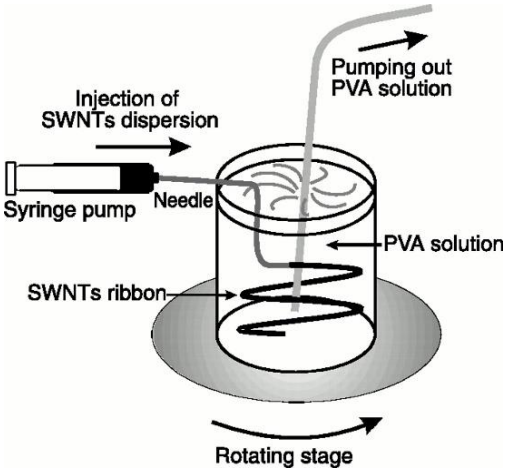

Figure 17: Schematic of the experimental setup used by Vigolo et al. to make CNT fibers. [32]

We pick this method because it allows us to easily dissolve the 2-TBB into the CNT solution. Once the CNT fiber is formed, the 2-TBB will be a part of the composite structure. Once current is passed through the fiber, the CNT junctions will form local hotspots. This should cause the 2-TBB in the structure to undergo thermal decomposition and the resulting all-carbon structure to covalently link the CNT junctions. Figure 18 depicts the process where the CNT junctions in the carbon nanotube fiber are nanosoldered.

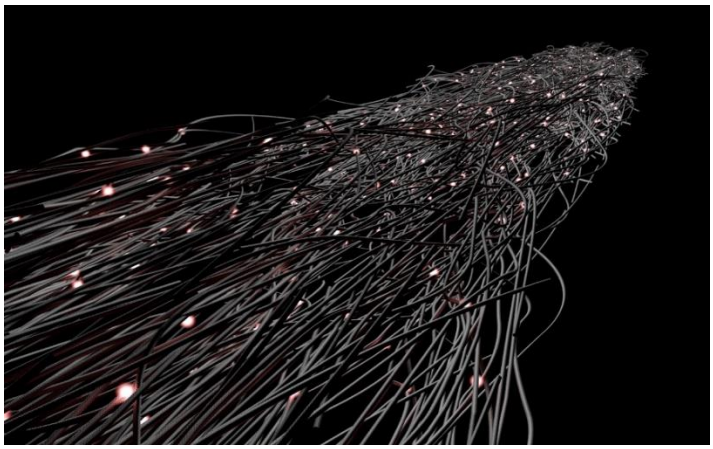

Figure 18: Schematic of the nanosoldering process occurring at the CNT junctions in the CNT fiber.

Image courtesy of Prof. Joseph Lyding (University of Illinois at Urbana-Champaign)

2.4 Experimental Procedure

For the purpose of our CNT fiber fabrication, we use CNTs synthesized through the high pressure carbon monoxide (HiPco) method. In this method, carbon monoxide (CO) is flowed at high temperatures (900 – 1100 °C) and high pressure (30 – 50 atm) into a CVD chamber on catalytic clusters of iron (Fe) [33]. CNTs grow from $Fe(CO)_5$ decomposition and condensation in the CO gas. A TEM image of HiPco CNTs can be seen in figure 19.

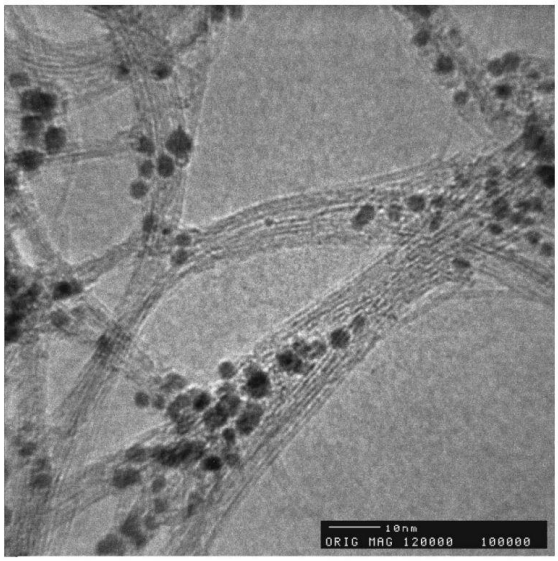

Figure 19: TEM image of CNTs grown using the HiPco process. Large catalyst particles can be seen in the image. [33]

In order to prepare the CNT solution, HiPco CNT powders were added to deionized water (DI H_2O) with a concentration of 4 mg/mL. Sodium cholate was used as a surfactant and added in concentrations of 2.5 mg/mL. The resulting solution is tip sonicated in an ice bath for 90 minutes.

The poly vinyl alcohol (PVA) solution was prepared by adding 20g of PVA powders to 230 mL of DI H_2O. The PVA solution is then heated at 100 °C for 3-4 hours and stirred occasionally. After that, it is set aside. Once the PVA solution has cooled to room temperature, it is ready for use.

The PVA solution is injected at a speed for 80 mL hr^{-1} to quickly fill up the quartz tube. Once the quartz tube is filled, the PVA solution injection speed is lowered to 30 mL hr^{-1}. After that, the CNT solution is injected at a speed of 0.25 mL hr^{-1}. Pictures of the experimental setup are shown in figure 20.

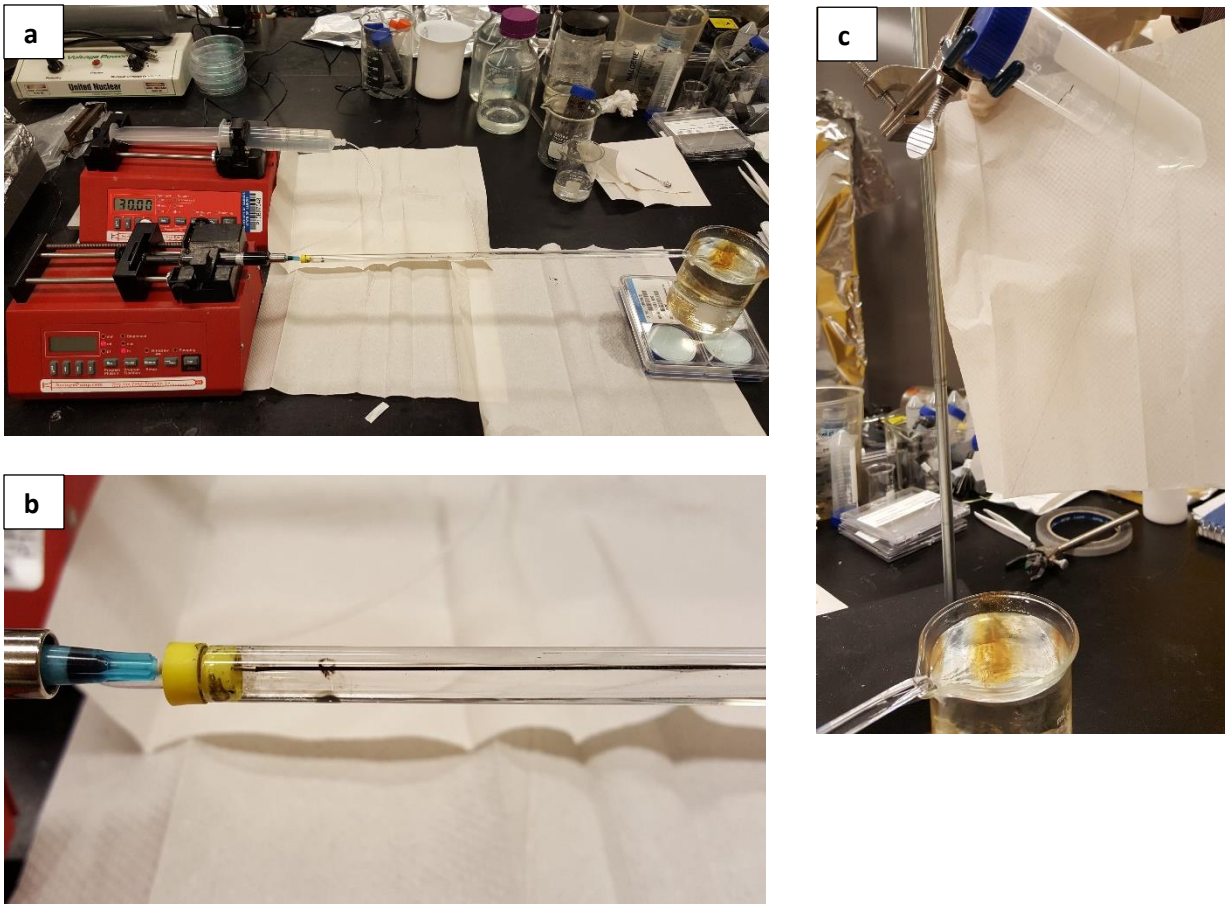

Figure 20: (a) Our experimental setup used to grow CNT fibers. (b) CNT solution coagulating into a fiber. (c) CNT fibers picked up and hung to dry after coagulation.

Once the CNT solution is streamed through the PVA solution, it coagulates into a fiber and it is picked up and hung to dry (figure 20 c). The fiber is left to dry for a few hours and after that it is characterized using Raman spectroscopy and scanning electron microscopy (SEM). An SEM image of the fiber is shown in figure 21 and a Raman spectrum is shown in figure 22.

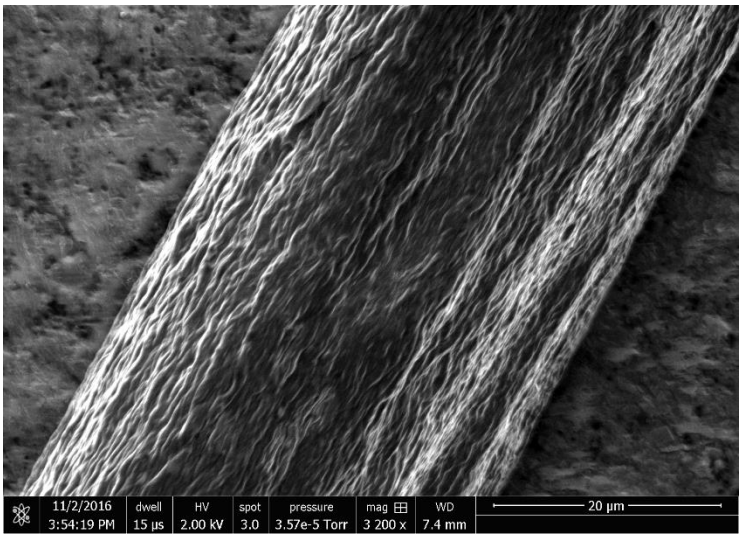

Figure 21: SEM image of a CNT fiber without 2-TBB (before nanosoldering).

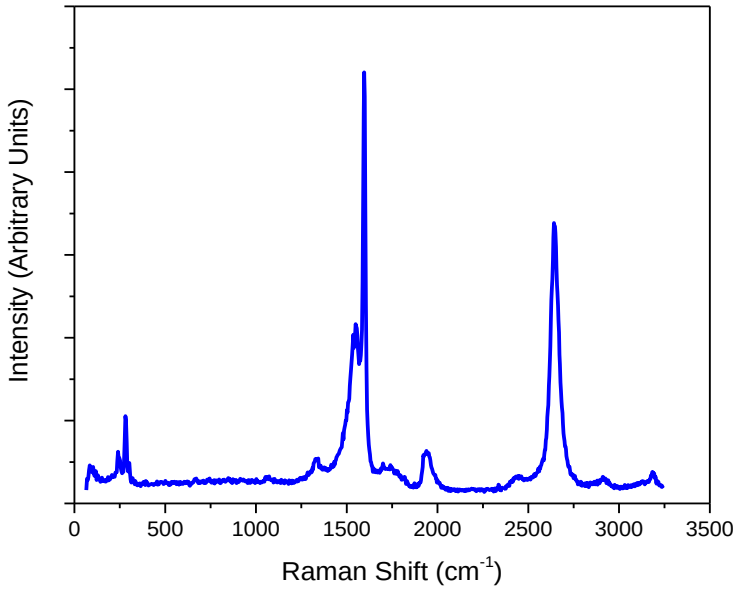

Figure 22: Raman spectrum of a CNT fiber without 2-TBB (before nanosoldering).

The SEM image in figure 21 indicates that our CNT fiber possesses a diameter of 30 μm. and the Raman spectrum in figure 22 shows the G and 2D peaks at ~1580 cm^{-1} and ~2700 cm^{-1} [34]. The D peak associated with defects is not visible and this tells us that our CNT fiber is of good quality.

In order to prepare CNT fibers with 2-TBB, the same procedure (described above) is repeated, but 20-30 mg of 2-TBB is added to the CNT solution. An SEM image of a CNT fiber with 2-TBB and a plot of its corresponding Raman spectrum are shown in figures 23, and 24.

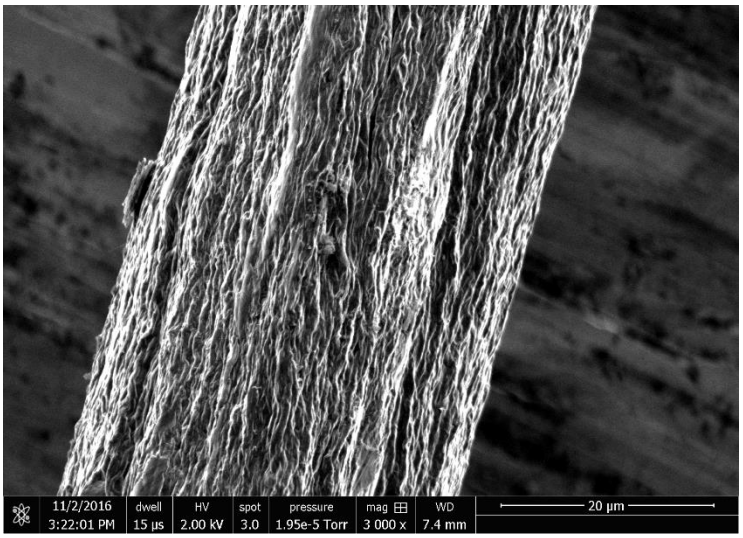

Figure 23: SEM image of a CNT fiber with 2-TBB (before nanosoldering).

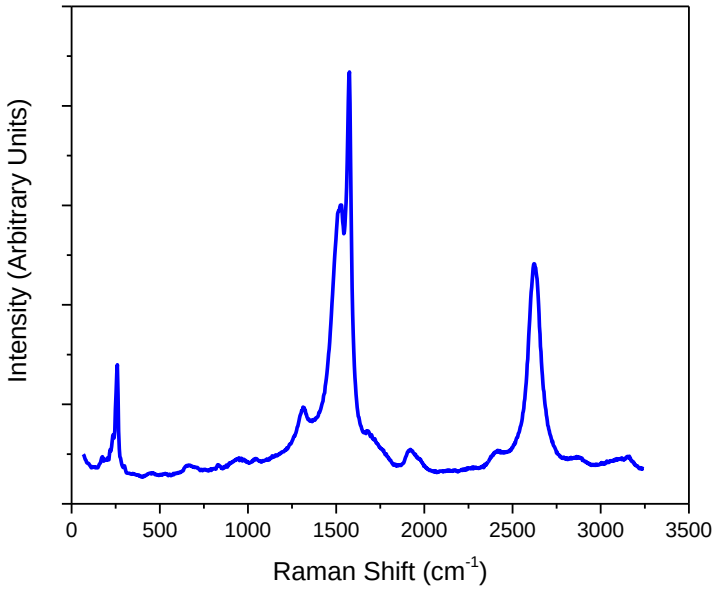

Figure 24: Raman spectrum of a CNT fiber with 2-TBB (before nanosoldering).

Figure 23 shows that the CNT fiber with 2-TBB also possesses a diameter of 30 μm and the corresponding Raman spectrum in figure 24 gives the peaks corresponding G and 2D peaks at ~1580 cm^{-1} and ~2700 cm^{-1}. These fibers are also of good quality.

Once the CNT fibers (with and without 2-TBB) were characterized and deemed to be of good quality, they were cut into smaller piece with lengths of ~ 12 – 15 cm. Individual fibers were then placed on a glass slide and coated with silver paint at four different points along the fiber. Copper wires were placed on these points and more silver paint was added to hold the copper wire in place. The glass slide setup can be seen in figure 25. The glass slide was then placed on a substrate holder (figure 25 a) and another glass slide was placed on top of it. A copper block is used to hold the glass slides in place. The final device structure can be seen in figures 25 a and b. This setup is loaded into the turbo chamber, shown in figure 25 (c), and pumped down to ~ 10^{-5} Torr.

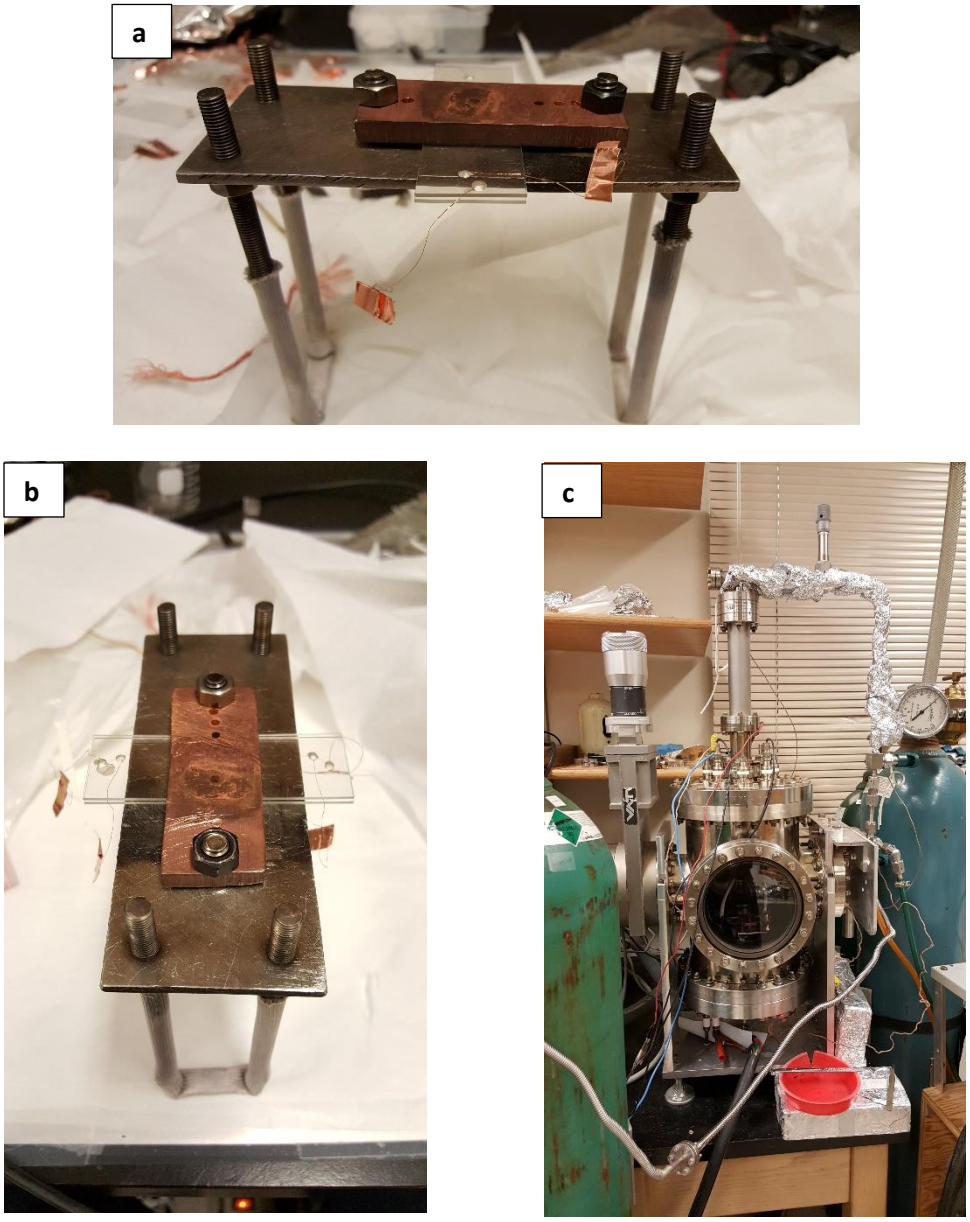

Figure 25: (a) Device structure used for the nanosoldering experiment (side view). (b) Top view of figure 25 (a). (c) Turbo chamber used for the nanosoldering experiment.

Electrical wires are connected to the turbo chamber leading to the substrate, creating a four-terminal sensing circuit. A schematic of the circuit can be seen in figure 26.

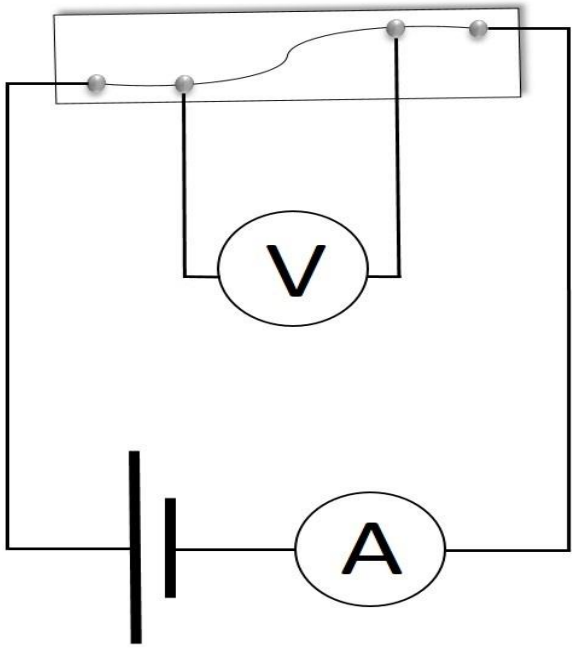

Figure 26: Schematic of the four-terminal sensing circuit used in the nanosoldering experiment.

Voltages were applied from 1 V and increased in 5 V increments up to ~ 140 V or when the limit of the power supply was reached. For each increment, we recorded the corresponding change in current. In section 2.5, we discuss the results of this technique. We compare the results of fibers with and without 2-TBB.

2.5 Results

The resistance of the fiber was calculated from the application of 1 V. Equation (1) was used with V and I being the measured voltages and current. With the resistance, the resistivity (ρ) was computed using equation (2) where L and A are the length of the fiber and the cross-sectional area. Finally, the conductivity (σ) was obtained by using equation (3). I-V curves of fibers with and without 2-TBB are shown in figure 27.

$$R = \frac{V}{I} \tag{1}$$

(2)

$$R = \rho \frac{L}{A}$$

(3)

$$\sigma = \frac{1}{\rho}$$

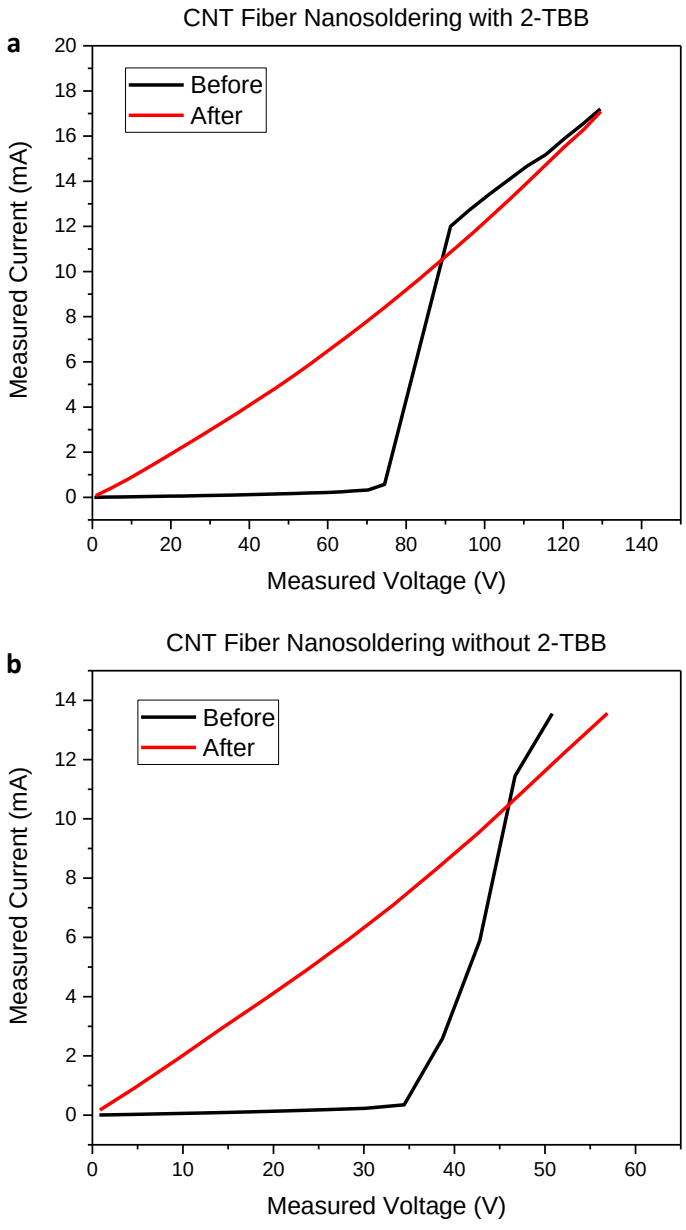

Figure 27: (a) I-V characteristics for a CNT fiber with 2-TBB. (b) I-V characteristics for a CNT fiber without 2-TBB.

After the fibers underwent nanosoldering in the turbo chamber, we performed Raman spectroscopy and used SEM to observe changes in the structure of the fiber. An SEM image of a CNT fiber after nanosoldering is displayed in figure 28 and a raman spectrum is shown in figure 29.

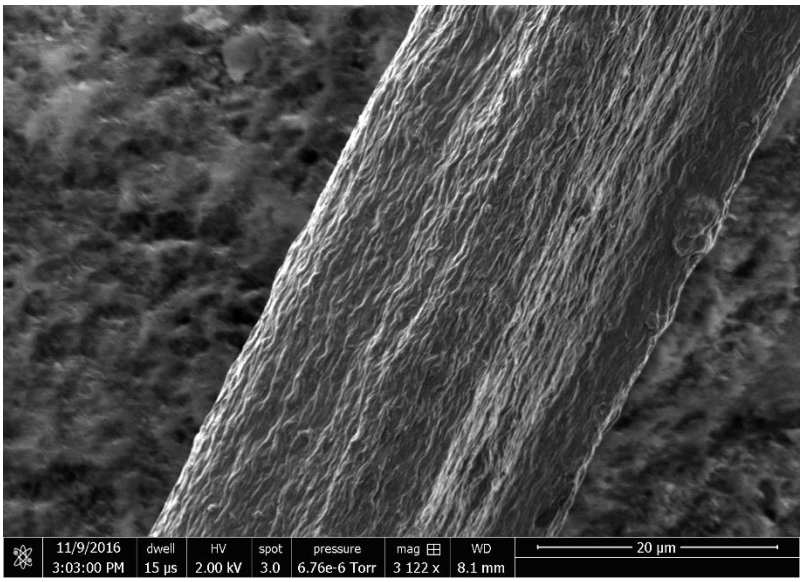

Figure 28*:* SEM image of a CNT fiber (after nanosoldering).

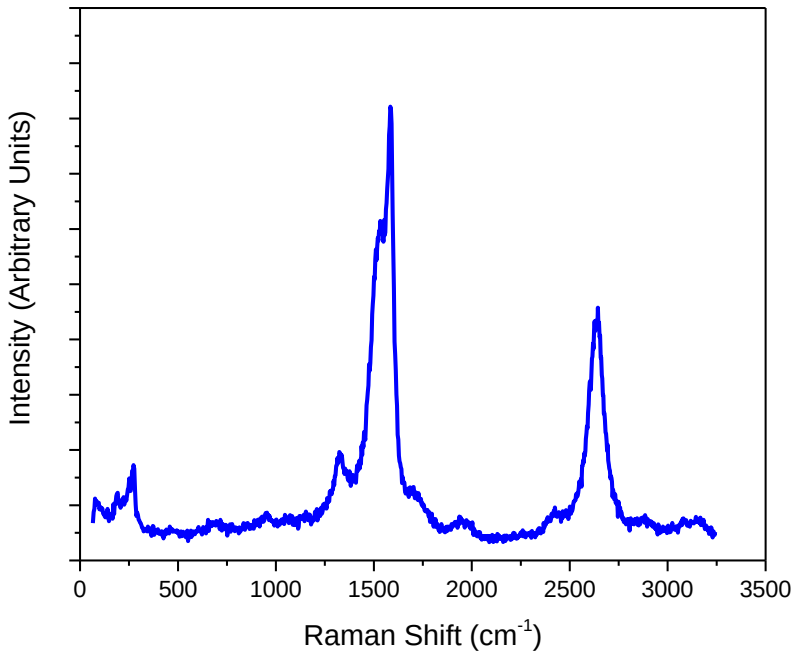

Figure 29*:* Raman spectrum of a CNT fiber (after nanosoldering).

SEM images of CNT fibers after nanosoldering show no change in the morphology and this is further corroborated by Raman spectroscopy. Referring to figure 29, the G and 2D peaks can be seen at ~1580 cm^{-1} and ~2700 cm^{-1}. This informs us that the nanosoldering does not change the physical structure of the CNT fiber.

The electrical conductivity of CNT fibers with 2-TBB improved from an average value of 157 ± 36 Sm^{-1} before nanosoldering to 10,190 ± 1670 Sm^{-1} after nanosoldering. The electrical conductivity of CNT fibers without 2-TBB improved from an average value of 176 ± 37 Sm^{-1} to 4869 ± 696 Sm^{-1}. While the conductivity values of the unsoldered fibers are in agreement with previous fabrication attempts [32], the conductivity values of the soldered fibers with 2-TBB are still lower than those reported by other sources [17].

It must be noted that fibers containing 2-TBB did display a significant improvement in electrical conductivity in comparison to fibers without the 2-TBB. We believe that the current heating is causing the 2-TBB to undergo thermal decomposition into the holey carbon structure that is linking individual nanotubes in the fibers. This covalent linking explains the improved conductivity which comes from the reduced resistance of the nanosoldered junctions.

In order to fully understand the effects of nanosoldering on the CNT fibers, we decided to measure the thermal conductivity of the CNT fibers before and after nanosoldering. Prof. Eric Pop's graduate student Feifei Lian at Stanford University performed the thermal conductivity measurements.

The measurements were performed using the technique described in Lian *et al.* [35] and the experimental setup is shown in figure 30. The temperature profile and IR images of an unsoldered and a soldered fiber are shown in figure 31.

The fibers were suspended at the contacts using silver paint. A voltage bias is applied to flow current through the fiber and an infrared (IR) scope is used to map the temperature in real time. To extract the thermal conductivity of the fiber, a finite element analysis of the 1D heat transfer equation [36] is used:

$$A\frac{\partial}{\partial y}\left(\kappa\frac{dT}{dy}\right) + p' - g[T(y) - T_0] = 0$$

A is the cross-sectional area of the film, κ is its in-plane thermal conductivity, and p' is joule heating power per unit length. The term g is the heat loss coefficient per unit length to the air or to the contacts and T_0 is the background temperature of the device. T(y) is the temperature at a location y along the fiber.

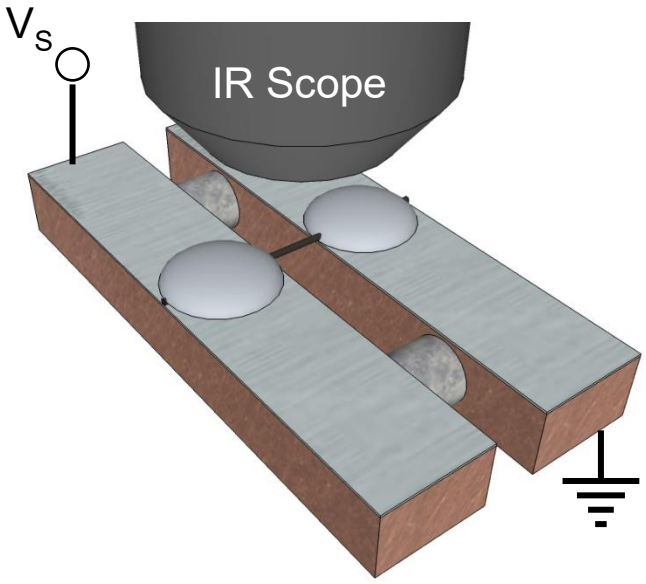

Figure 30: Experimental setup used by Feifei Lian to measure the thermal conductivity of the CNT fibers

Image courtesy of Feifei Lian (Stanford University)

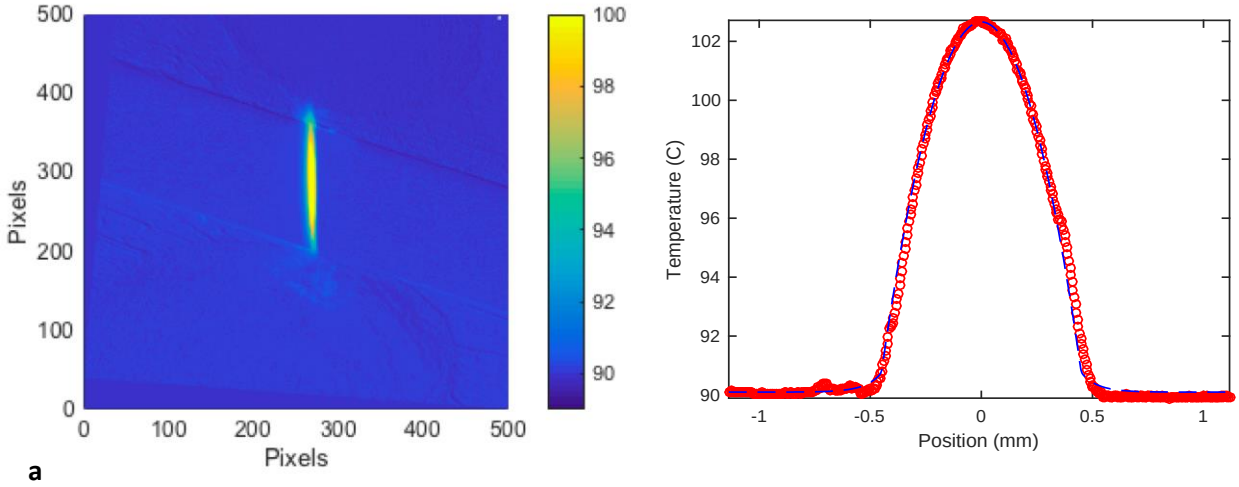

Unsoldered CNT fiber: $\kappa = 40$

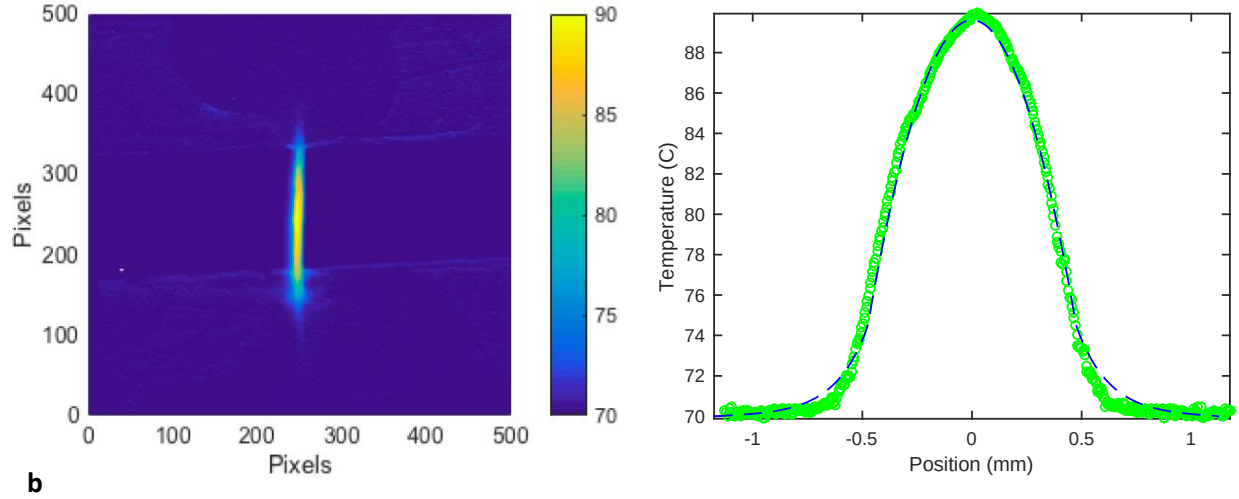

Soldered CNT fiber: $\kappa = 100$

Figure 31: (a) IR image and temperature profile of an unsoldered CNT fiber. (b) IR image and temperature profile of a soldered CNT fiber.

Images courtesy of Feifei Lian (Stanford University)

The unsoldered fibers possessed a thermal conductivity of ~ 40 – 60 $Wm^{-1}K^{-1}$. Unfortunately, the nanosoldered fibers with 2-TBB witnessed a reduction in thermal conductivity to ~ 15 – 30 $Wm^{-1}K^{-1}$. The best result, displayed in figure 31 (b), showed a thermal conductivity of ~ 100 $Wm^{-1}K^{-1}$. Since these fibers are ~40% PVA, we believe that the nanosoldering thermally decomposes the PVA causing amorphous carbon to form along the fibers [37]. The thermal conductivity of amorphous carbon thin films ranges from 0.2 to 2.2 $Wm^{-1}K^{-1}$ [38]. The formation

of the amorphous carbon along the fiber explains the reduction in thermal conductivity after nanosoldering.

2.6 Discussions

In the work described in this chapter, we fabricated CNT fibers and applied the nanosoldering technique our group developed for CNT FETs. The purpose of this experiment was to use the nanosoldering process to strengthen the CNT fibers (electrically and thermally). While the electrical conductivity of CNT fibers with 2-TBB improved from 157 ± 36 Sm^{-1} before nanosoldering to 10,190 ± 1670 Sm^{-1} after nanosoldering, the thermal conductivity essentially decreased. With the exception of a single fiber which improved to 100 $Wm^{-1}K^{-1}$, most fibers witnessed a reduction from ~ 40 - 60 $Wm^{-1}K^{-1}$ to ~ 15 – 30 $Wm^{-1}K^{-1}$.

We attribute these results to the PVA in the fibers. The PVA is a polymeric insulating material that could be limiting the effects of nanosoldering and the potential improvement in electrical and thermal properties. To overcome this challenge, future work should be centered on producing polymer-free CNT fibers that could display greatly enhanced properties after the nanosoldering process.

2.7 References

[1] L. Hu, D. S. Hecht, and G. Grüner, "Percolation in transparent and conducting carbon nanotube networks," *Nano Letters*, vol. 4, no. 12, pp. 2513–2517, Oct. 2004.

[2] P. N. Nirmalraj, P. E. Lyons, S. De, J. N. Coleman, and J. J. Boland, "Electrical connectivity in single-walled carbon nanotube networks," *Nano Letters*, vol. 9, no. 11, pp. 3890–3895, Sep. 2009.

[3] M. Stadermann et al., "Nanoscale study of conduction through carbon nanotube networks," *Physical Review B*, vol. 69, no. 20, p. 201402, May 2004.

[4] S. Kumar, M. A. Alam, and J. Y. Murthy, "Effect of percolation on thermal transport in nanotube composites," *Applied Physics Letters*, vol. 90, no. 10, p. 104105, Mar. 2007.

[5] A. V. Kyrylyuk, "Controlling electrical percolation in multicomponent carbon nanotube dispersions," *Nature Nanotechnology*, vol. 6, no. 6, pp. 364–369, Apr. 2011.

[6] M. S. Fuhrer et al., "Crossed nanotube junctions," *Science*, vol. 288, no. 5465, pp. 494–497, Apr. 2000.

[7] M. A. Alam, N. Pimparkar, S. Kumar, and J. Murthy, "Theory of nanocomposite network transistors for macroelectronics applications," *MRS Bulletin*, vol. 31, no. 6, pp. 466–470, Jun. 2006.

[8] H. Zhong and J. R. Lukes, "Interfacial thermal resistance between carbon nanotubes: Molecular dynamics simulations and analytical thermal modeling," *Physical Review B*, vol. 74, no. 12, p. 125403, Sep. 2006.

[9] R. S. Prasher et al., "Turning carbon nanotubes from exceptional heat conductors into insulators," *Physical Review Letters*, vol. 102, no. 10, p. 105901, Mar. 2009.

[10] J. Yang, S. Waltermire, Y. Chen, A. A. Zinn, T. T. Xu, and D. Li, "Contact thermal resistance between individual multiwall carbon nanotubes," *Applied Physics Letters*, vol. 96, no. 2, p. 023109, Jan. 2010.

[11] D. Estrada and E. Pop, "Imaging dissipation and hot spots in carbon nanotube network transistors," *Applied Physics Letters*, vol. 98, no. 7, p. 073102, Feb. 2011.

[12] G. Shen, Y. Lu, L. Shen, Y. Zhang, and S. Guo, "Nondestructively creating nanojunctions by combined-dynamic-mode dip-pen nanolithography," *ChemPhysChem*, vol. 10, no. 13, pp. 2226–2229, Jul. 2009.

[13] M. S. Wang, J. Y. Wang, Q. Chen, and L. –M.Peng, "Fabrication and electrical and mechanical properties of carbon nanotube interconnections," *Advanced Functional Materials*, vol. 15, no. 11, pp. 1825–1831, Sep. 2005.

[14] J.-W. Do et al., "Nanosoldering carbon nanotube junctions by local chemical vapor deposition for improved device performance," *Nano Letters*, vol. 13, no. 12, pp. 5844–5850, Nov. 2013.

[15] J.-W. Do et al., "Solution-mediated selective nanosoldering of carbon nanotube junctions for improved device performance," *ACS Nano*, vol. 9, no. 5, pp. 4806–4813, Apr. 2015.

[16] J.-W. Do, "Selective metallization and electronic self-healing for high performance carbon-based nanoelectronics," Ph.D. Dissertation, University of Illinois at Urbana-Champaign, Urbana, IL, Apr. 2015.

[17] A. Lekawa-Raus, J. Patmore, L. Kurzepa, J. Bulmer, and K. Koziol, "Electrical properties of carbon nanotube based fibers and their future use in electrical wiring," *Advanced Functional Materials*, vol. 24, no. 24, pp. 3661–3682, Mar. 2014.

[18] N. Behabtu, M. J. Green, and M. Pasquali, "Carbon nanotube-based neat fibers," *Nanotoday*, vol. 3, no. 5–6, pp. 24–34, Oct. 2008.

[19] R. H. Baughman, A. A. Zakhidov, and W. A. de Heer, "Carbon Nanotubes--the route toward applications," *Science*, vol. 297, no. 5582, pp. 787–792, Aug. 2002.

[20] A. Jorio, G. Dresselhaus, and M. S. Dresselhaus, *Carbon Nanotubes: Advanced Topics in the Synthesis, Structure, Properties and Applications*, A. Jorio, G. Dresselhaus, and M. S. Dresselhaus, Eds., 2001st ed. Germany: Springer, 2008.

[21] R. M. Sundaram, K. K. K. Koziol, and A. H. Windle, "Continuous direct spinning of fibers of single-walled carbon nanotubes with metallic chirality," *Advanced Materials*, vol. 23, no. 43, pp. 5064–5068, Oct. 2011.

[22] Y.-L. Li, I. A. Kinloch, and A. H. Windle, "Direct spinning of carbon nanotube fibers from chemical vapor deposition synthesis," *Science*, vol. 304, no. 5668, pp. 276–278, Apr. 2004.

[23] H. W. Zhu, C. L. Xu, D. H. Wu, B. Q. Wei, R. Vajtai, and P. M. Ajayan, "Direct synthesis of long single-walled carbon nanotube strands," *Science*, vol. 296, no. 5569, pp. 884–886, May 2002.

[24] X.-H. Zhong et al., "Continuous multilayered carbon nanotube yarns," *Advanced Materials*, vol. 22, no. 6, pp. 692–696, Nov. 2009.

[25] M. Zhang, K. R. Atkinson, and R. H. Baughman, "Multifunctional carbon nanotube yarns by downsizing an ancient technology," *Science*, vol. 306, no. 5700, pp. 1358–1361, Nov. 2004.

[26] M. Miao, "Electrical conductivity of pure carbon nanotube yarns," *Carbon*, vol. 49, no. 12, pp. 3755–3761, May 2011.

[27] X. Zhang et al., "Strong carbon-nanotube fibers spun from long carbon-nanotube arrays," *Small*, vol. 3, no. 2, pp. 244–248, Jan. 2007.

[28] L. Zheng et al., "Carbon-nanotube cotton for large-scale fibers," *Advanced Materials*, vol. 19, no. 18, pp. 2567–2570, Aug. 2007.

[29] L. Ci, N. Punbusayakul, J. Wei, R. Vajtai, S. Talapatra, and P. M. Ajayan, "Multifunctional macroarchitectures of double-walled carbon nanotube fibers," *Advanced Materials*, vol. 19, no. 13, pp. 1719–1723, Jun. 2007.

[30] W. Ma et al., "Monitoring a micromechanical process in macroscale carbon nanotube films and fibers," *Advanced Materials*, vol. 21, no. 5, pp. 603–608, Dec. 2008.

[31] W. Ma et al., "Directly synthesized strong, highly conducting, transparent single-walled carbon nanotube films," *Nano Letters*, vol. 7, no. 8, pp. 2307–2311, Jul. 2007.

[32] B. Vigolo et al., "Macroscopic fibers and ribbons of oriented carbon nanotubes," *Science*, vol. 290, no. 5495, pp. 1331–1334, Nov. 2000.

[33] M. J. Bronikowski, P. A. Willis, D. T. Colbert, K. A. Smith, and R. E. Smalley, "Gas-phase production of carbon single-walled nanotubes from carbon monoxide via the HiPco process: A parametric study," *Journal of Vacuum Science & Technology A: Vacuum, Surfaces, and Films*, vol. 19, no. 4, pp. 1800–1805, Jul. 2001.

[34] M. S. Dresselhaus, G. Dresselhaus, R. Saito, and A. Jorio, "Raman spectroscopy of carbon nanotubes," *Physics Reports*, vol. 409, no. 2, pp. 47–99, Feb. 2005.

[35] F. Lian, J. P. Llinas, Z. Li, D. Estrada, and E. Pop, "Thermal conductivity of chirality-sorted carbon nanotube networks," *Applied Physics Letters*, vol. 108, no. 10, p. 103101, Mar. 2016.

[36] E. Pop, D. A. Mann, K. E. Goodson, and H. Dai, "Electrical and thermal transport in metallic single-wall carbon nanotubes on insulating substrates," *Journal of Applied Physics*, vol. 101, no. 9, p. 093710, May 2007.

[37] Y. Tsuchiya and K. Sumi, "Thermal decomposition products of poly(vinyl alcohol)," *Journal of Polymer Science Part A-1: Polymer Chemistry*, vol. 7, no. 11, pp. 3151–3158, Nov. 1969.

[38] A. J. Bullen, K. E. O'Hara, D. G. Cahill, O. Monteiro, and A. von Keudell, "Thermal conductivity of amorphous carbon thin films," *Journal of Applied Physics*, vol. 88, no. 11, pp. 6317–6320, Nov. 2000.

[39] L. M. Ericson et al., "Macroscopic, neat, single-walled carbon nanotube fibers" *Science*, vol. 305, no. 5689, pp. 1447–1450, Sep. 2004.

3. Graphene Nanoribbon Thin Film Transistors

3.1 Synthesis and Processing of Graphene Nanoribbons for Device Studies

As mentioned in chapter 1, the lack of a band gap makes graphene unsuitable for digital electronics. As graphene is thinned down to widths ~10 nm and smaller, quantum confinement induces a band gap. This material, a graphene nanoribbon (GNR), holds great promise for electronic applications.

Exploring the potential of graphene nanoribbons is difficult because of the challenges associated with synthesis. While GNRs can be synthesized using chemical [1-3], sonochemical [4], and lithographic techniques [5, 6], and through the unzipping of carbon nanotubes (CNTs) [7-10], these methods do not guarantee atomic precision. The ability to produce GNRs with atomic precision is the key to practical realization of their electronic properties. AFM images of a chemically derived GNR and the process for unzipping CNTs are shown in figures 32 and 33.

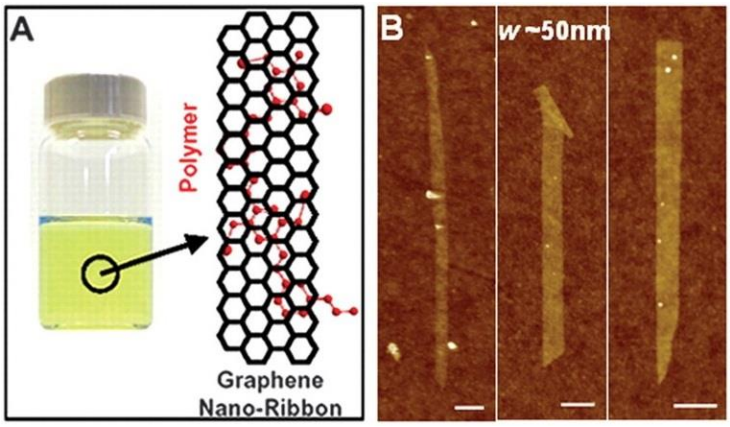

Figure 32: (A) Photograph of a polymer PmPV/DCE solution with GNRs suspended in the solution. (B) AFM image of GNRs that are 50 nm wide. Scale bar is 100 nm. [4]

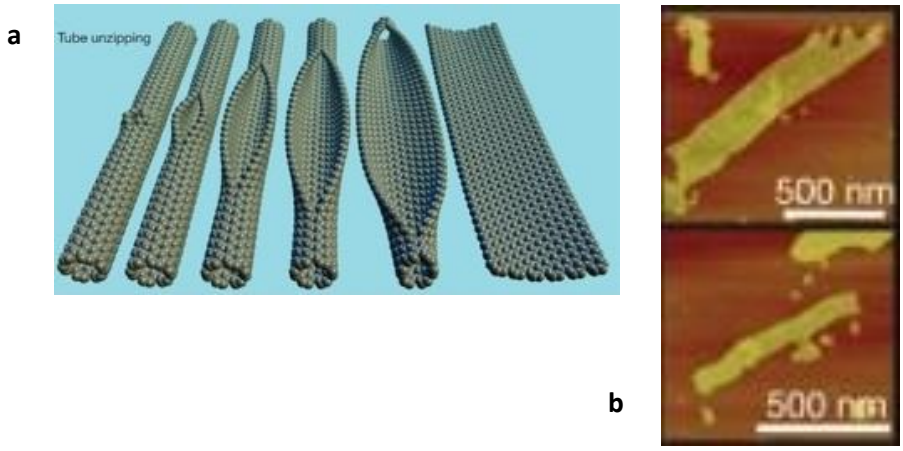

Figure 33: (a) Schematic illustration of the unzipping of a carbon nanotube to form a graphene nanoribbon. (b) AFM images of graphene nanoribbons after the unzipping process. [8]

The bottom-up approach developed by Cai et al. uses surface-assisted coupling of molecular precursors into linear polyphenylenes and their subsequent cyclodehydrogenation to produce GNRs with atomic precision [11]. The process and a high-resolution image of the GNRs are shown in figure 34. Likewise, several types of atomically precise GNRs with different geometries and widths have been synthesized in solution and on metal surfaces [12-14]. Regardless of the progress achieved in the solution synthesis of atomically precise GNRs, their device studies have been minimal [15-18].

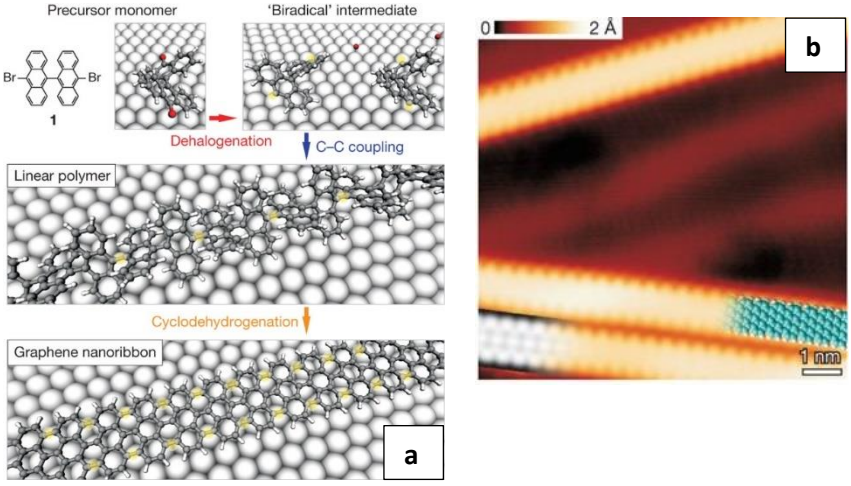

Figure 34: (a) Schematic illustration for the basic steps in GNR synthesis. (b) High-resolution STM image of the GNRs after the cyclodehydrogenation step. [11]

One of the greatest challenges hindering electrical characterization of atomically precise GNRs is the lack of simple and effective processing techniques. GNRs that are synthesized on growth substrates such as Au (111) require transfer to a target device substrate, which is complicated and often of poor quality. Likewise, solution synthesized GNRs are equally difficult to transfer because of their aggregation, entanglement and poor solubility in organic solvents.

One approach to increasing the solubility of polyaromatic molecules is by functionalizing their edges with alkyl chains as this should improve their processability. This approach was applied to some of the solution synthesized GNRs [19, 20]. While this technique might prove advantageous, the alkyl chains might affect GNR assembly which would reduce the number of contacts between GNRs and impair the electronic properties of the bulk material.

Another approach would be the use of surfactants. This technique was previously used to prepare solutions and suspensions of graphene [21]. Even if this technique were applied to GNRs, like the alkyl chains, the surfactants can decrease the volume fraction of GNRs in the bulk material and reduce electrical conductivity.

The problems associated with these processing techniques create a need for a method that can dissolve atomically precise GNRs in solvents without adding surfactants or alkyl chains that would otherwise damage either electronic properties. In this chapter, a new fabrication approach for large-scale uniform thin films of non-functionalized atomically precise GNRs is proposed. These GNR thin films are subsequently used as the channel material for transistor fabrication and the resulting devices are characterized.

3.2 Experimental Procedure

The GNRs used in this thesis were synthesized by Vo et al. and are 1 nm wide with uniform armchair edges [22]. The procedure utilized the polymerization of pre-synthesized molecular

precursors by a Ni^0-mediated Yamamoto coupling [23] followed by a cyclodehydrogenation via Scholl reaction using iron (III) chloride [24] into GNRs. The reaction scheme is shown in figure 35 (c) and an STM image of the GNR is shown in figure 35 (d).

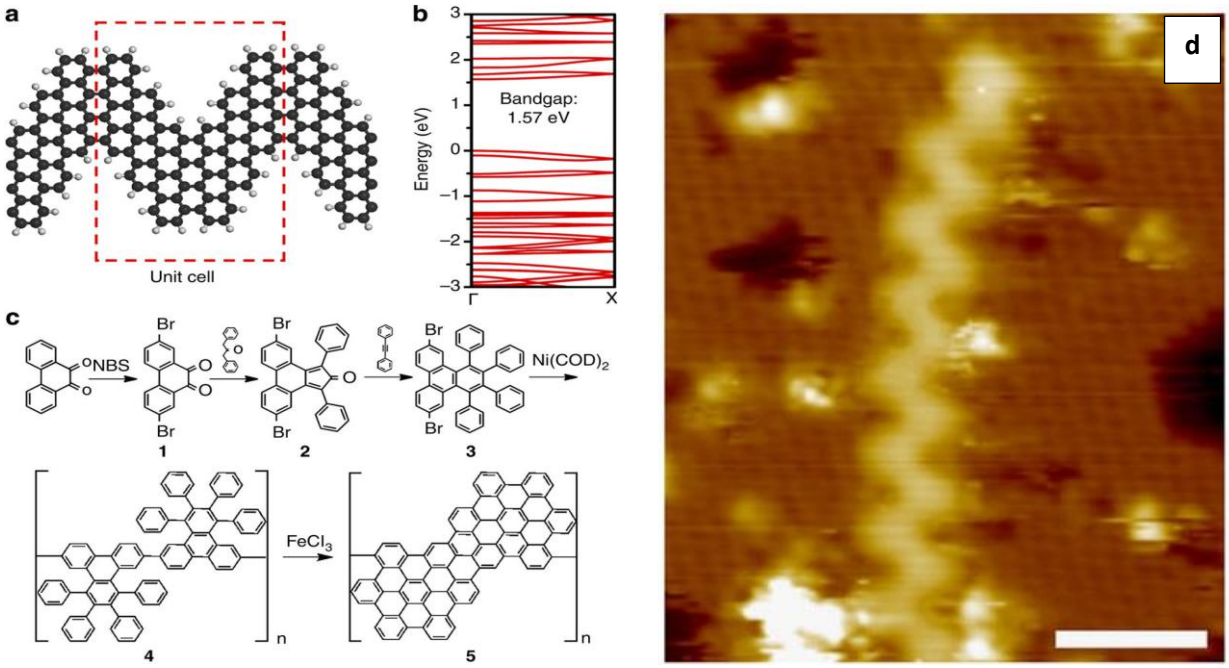

Figure 35: (a) Schematic of the GNR synthesized by Vo et al. (b) Corresponding calculated band structure. (c) Reaction scheme for the GNR synthesis. (d) STM image of the GNR on Au (111). Scale bar is 3 nm. [22]

These GNRs were dissolved in chlorosulfonic acid (CSA) with a concentration of 3.75 mg/mL. CSA was chosen because it was previously shown to be an effective solvent for various graphitic materials such as SW CNTs [25] and graphite [26]. The thin films were fabricated by taking advantage of the fact that the GNRs are insoluble in most solvents other than CSA. When the GNRs are transferred from the CSA to the surface of another solvent, they minimize their interaction with the solvent by forming a densely packed self-assembled and layered film.

The GNR solution is pipetted along a glass slide, which is half immersed into a tall beaker of DI H_2O. Once the solution reaches the surface of the DI H_2O, the CSA reacts instantly with the DI H_2O forming sulfuric and hydrochloric acids. This leaves the hydrophobic GNRs at the liquid-air interface. They self-assemble via π - π stacking to minimize their interactions with the solvent and maximize their interactions with each other. The result of this is a densely packed self-assembled and layered film. The process is highlighted in figure 36.

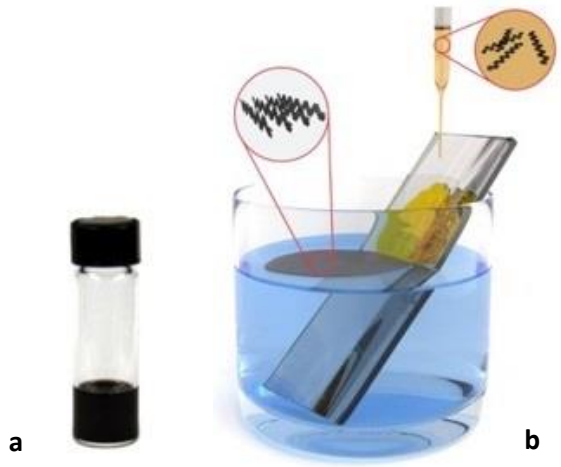

Figure 36: (a) Picture of a vial with the solution of GNRs in CSA. (b) Schematic illustration of the interfacial self-assembly approach, by pipetting the CSA-GNR solution into water. [3]

The thin film is fished out with another glass slide and transferred to another beaker with DI H_2O to wash away acid residues. The washing procedure is repeated several times and the GNR film is fished out by a SiO_2/Si substrate with pre-patterned metal contacts for electrical characterization.

The metal contacts were prepared by thermal evaporation of 0.6 nm titanium (Ti) and 80 nm palladium (Pd) onto the SiO_2/Si substrate with gaps ranging from 2 um to ~80um. When the GNR film was fished out, it was done to cover the entire substrate area with the Ti/Pd electrodes.

The device channels were patterned using ultraviolet (UV) lithography and the GNRs outside of the channels were etched away with O_2 plasma. The O_2 plasma etch was performed at 100 mTorr, with 20 sccm O_2 at 100 watts for 60 seconds. The sample was subsequently placed in a solvent stripper (Remover PG) and rinsed with isopropanol (IPA). The purpose of the etch was to create individual transistor devices and prevent a continuous GNR film from short circuiting the device. A schematic of an individual GNR thin film transistor is shown in figure 37 (a) and SEM images of the actual devices are shown in figures 37 (b) and 37 (c). The actual transistor channel is comprised of multiple π-π stacked GNRs that are randomly oriented with each other.

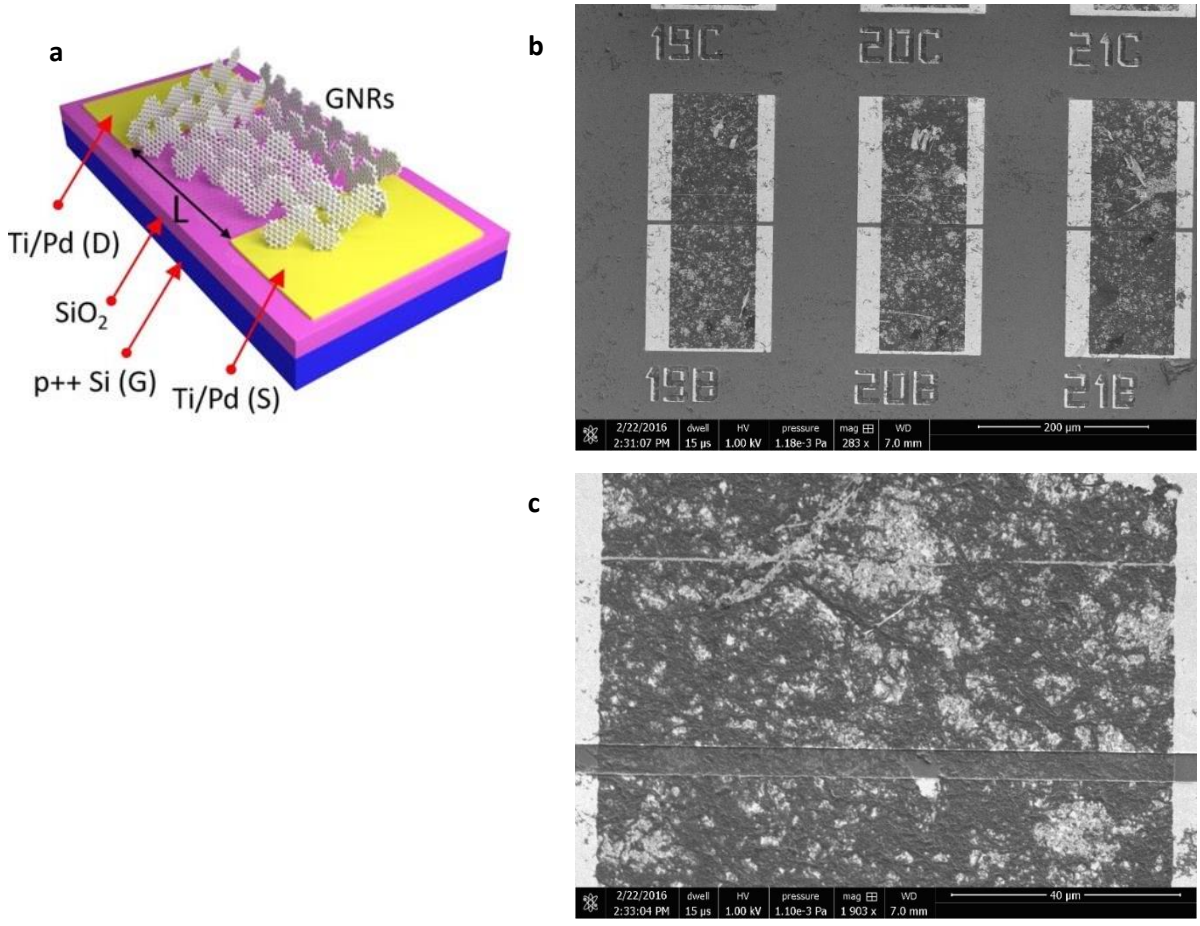

Figure 37: (a) Schematic of a GNR thin film transistor. [3] (b) SEM image of three GNR thin film transistors. (c) Magnified SEM image of a GNR thin film transistor.

The samples were annealed twice in a tube furnace in order to remove contaminants and residues from the processing steps. The first anneal occurred in vacuum at 300 °C for 1 hr and the second in vacuum in a Ar/H_2 atmosphere at 300 °C for 1 hr. The flow rate for the Ar and H_2 was 400 sccm.

The devices were tested in air using a Keithley 4200-SCS semiconductor analyzer. All measurements were done before and after each annealing procedure. The tube furnace used for the annealing is shown in figure 38 (a) and the Keithley tool used for electrical measurements is shown in figure 38 (b).

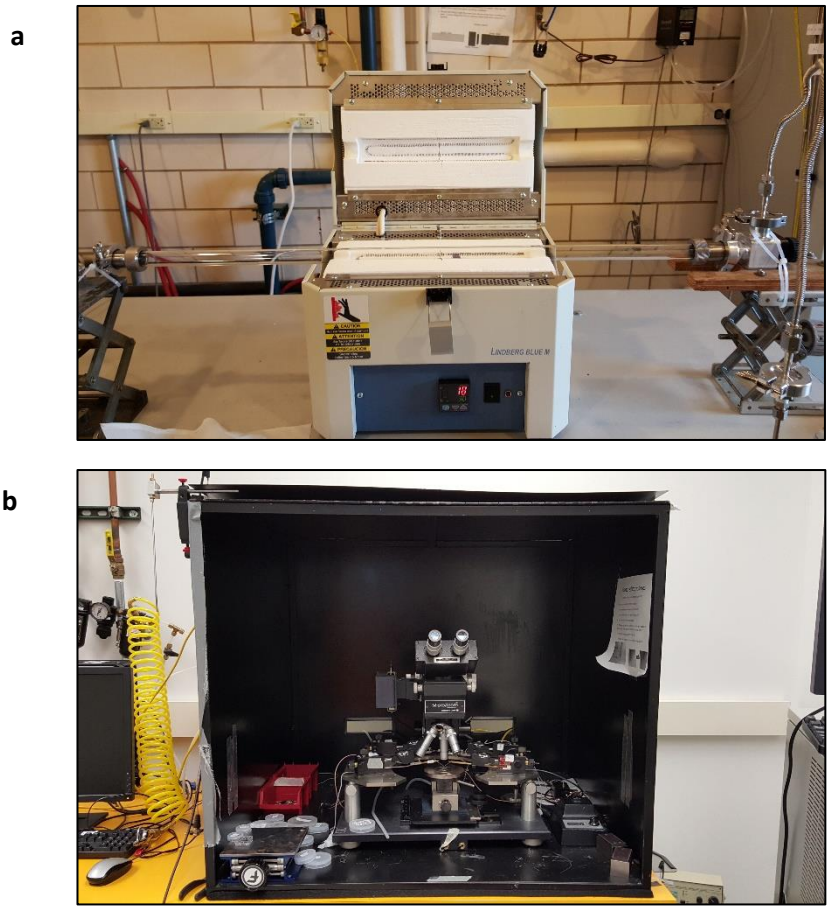

Figure 38: (a) Tube furnace in MRL used for annealing procedures. (b) Keithley 4200-SCS semiconductor analyzer in MNTL used for characterizing the GNR thin film transistors.

3.3 Results

After the GNR thin film was fished out by the SiO2/Si substrate with pre-patterned metal Contacts, we performed a Raman measurement to verify the quality of the GNRs. The Raman spectrum can be seen in figure 39 (a). Likewise, we performed another Raman spectrum after the two annealing procedures to ensure that the GNRs were not damaged during this process. The Raman spectrum after the annealing procedures is displayed in figure 39 (b).

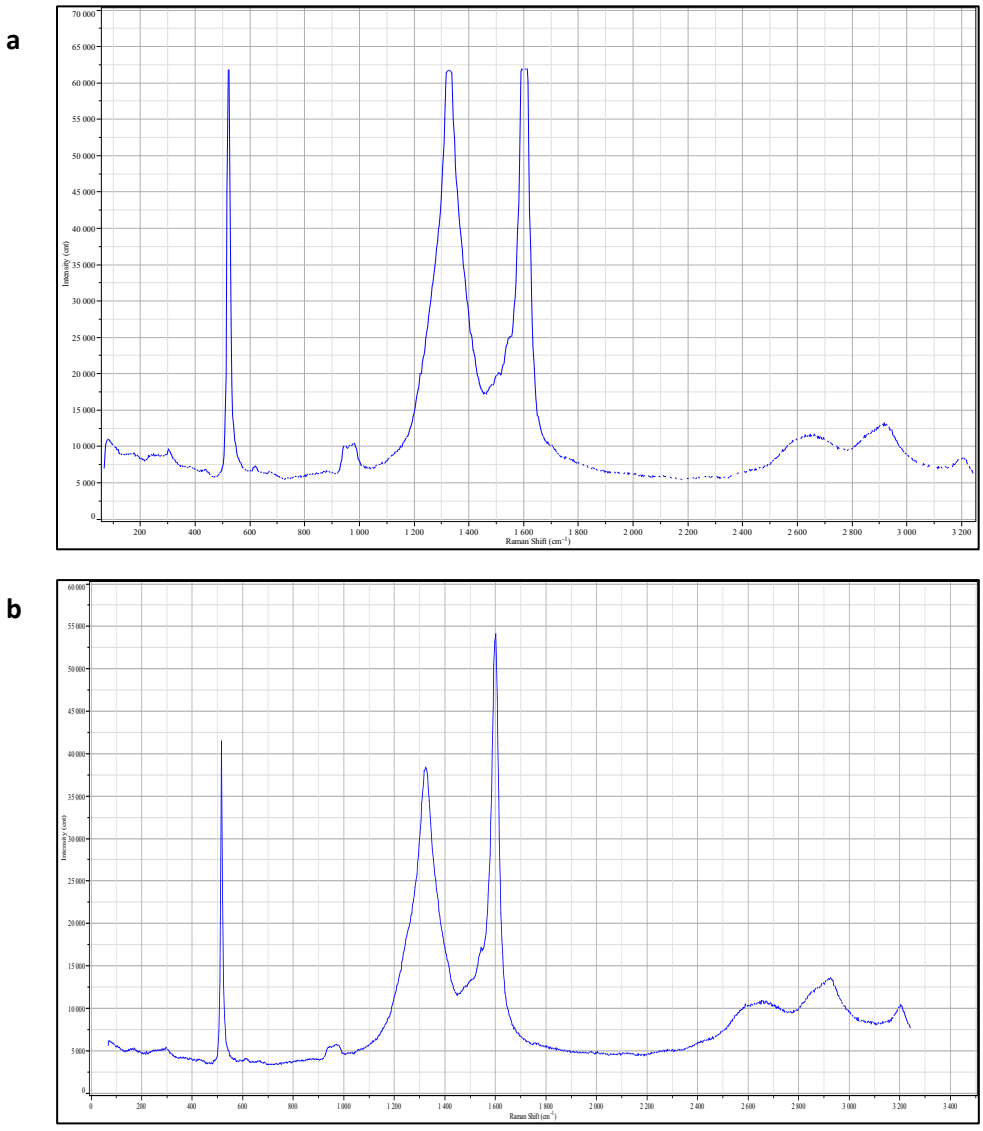

Figure 39: (a) Raman spectroscopy of the GNR thin film transistors before the annealing procedure. (b) Raman spectroscopy of the GNR thin film transistors after the annealing procedure.

The most intense lines corresponding to GNRs can be seen at ~1300 and ~1600 cm^{-1} in both figures 36 and 37. These are the D and G bands [27]. The peak at ~500 cm^{-1} corresponds to the SiO_2 substrate. It is interesting to note the reduction in the D peak in figure 37 as compared to figure 36. We believe that the reduction in the D peak is caused by the two annealing procedures. The annealing procedures serve to remove residues and contaminants from the processing steps and restore the structure of the GNRs. The D/G peak ratio in figure 37 agrees with the Raman characterization of the original GNRs after synthesis described by Vo et al. [22]. The Raman spectrum of the GNRs (after synthesis) is displayed in figure 40.

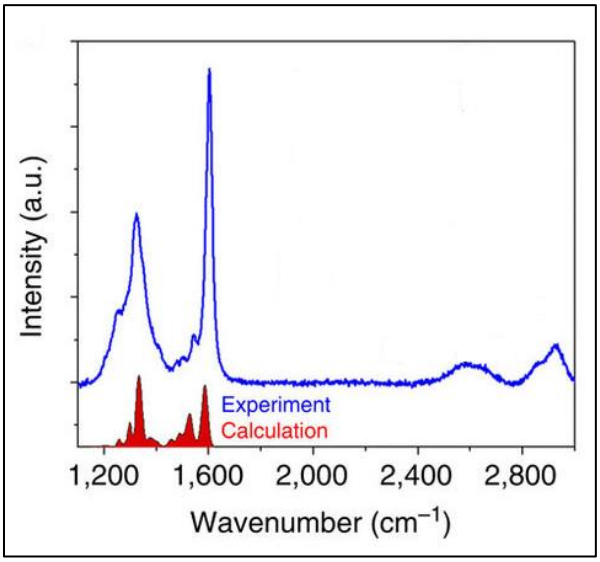

Figure 40: (a) Raman spectroscopy of the GNRs after synthesis. [22]

The electronic properties of the GNR based devices are shown in figure 41.

.

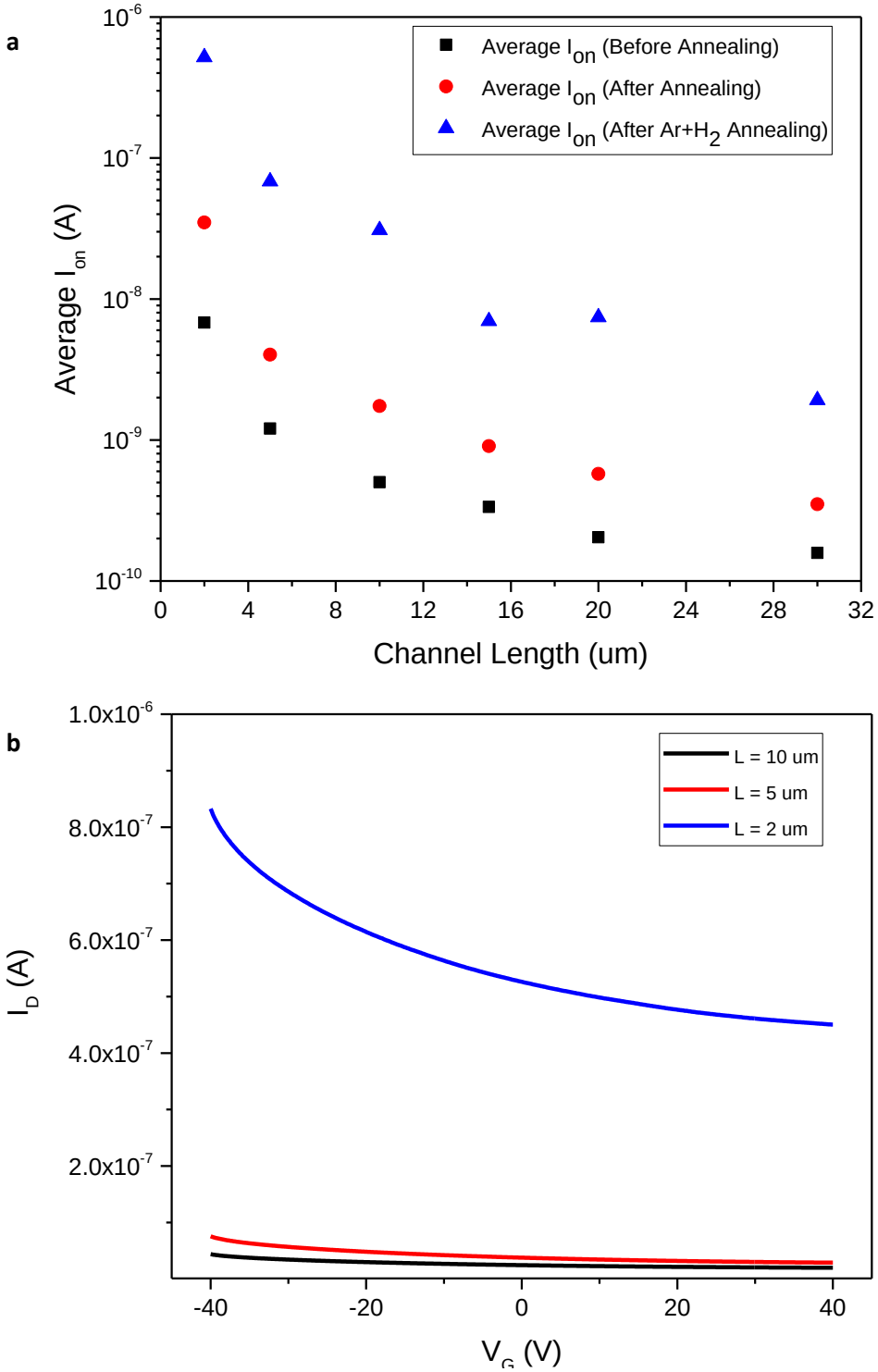

Figure 41: (a) Average I_{on} of the GNR thin film transistors after the processing steps with respect to channel length. (b) I-V characteristics of the GNR thin film transistors for channel lengths (L = 2, 5, and 10 μm). Continued on next page.

c

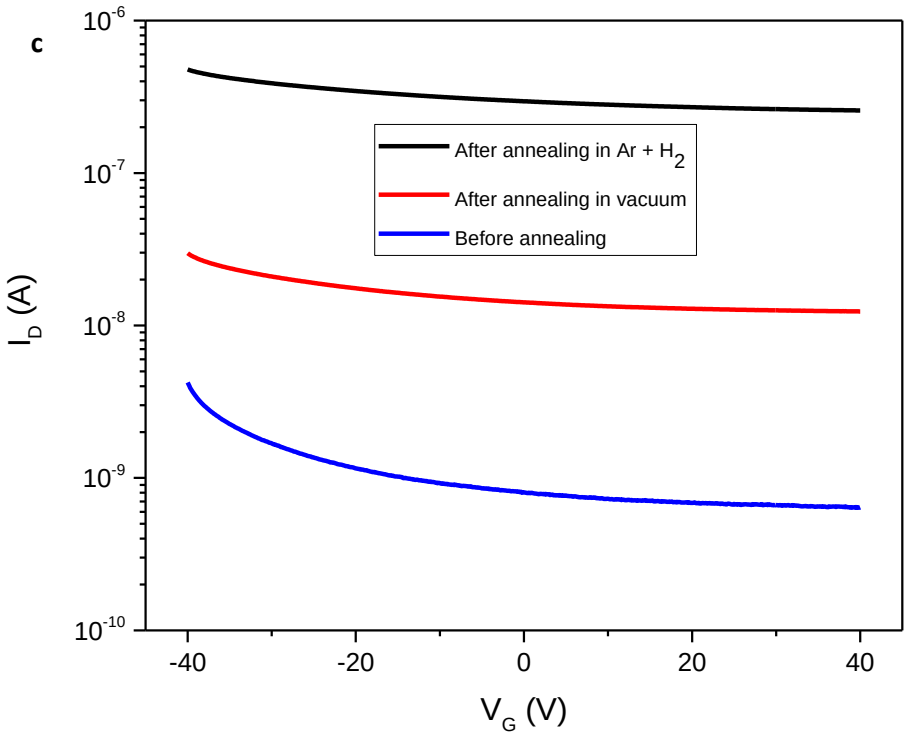

d

Processing Step	Average I_{on}/I_{off} Ratio	Average I_{on} (nA)
Before annealing	8.97	9.41
After annealing in vacuum	4.21	46.06
After annealing in Ar + H_2	3.04	832.57

Figure 41 (continued): (c) I-V characteristics of an L = 2 μm GNR thin film transistor after the various processing steps. (d) Table showing the average I_{on}/I_{off} ratio and average I_{on} after each processing step.

Electrical measurements in figure 41 (b) and (c) showed that the devices exhibit p-type behavior with gate modulated conductance. Considering that the source-drain distances (L) varied from 2 μm to 30 μm, and the GNRs are less than 100 nm long, the electrical measurements probed the GNR films and also the inter-GNR junctions. Figure 41 (a) shows increasing conductivity with decreasing channel lengths. This can also be seen in figure 41 (b) which shows the $I_D - V_G$ curves of L = 2, 5 and 10 μm devices. We attribute the improvement in conductivity to the smaller number of inter-GNR junctions in the shorter channel devices. These results encourage future studies into even shorter channel length GNR devices.

For the purpose of this experiment, we also studied the effects of the annealing procedures on the electrical performance on the GNR devices. After annealing in vacuum at 300 °C, the average on currents (I_{on}) improved from 9.41 nA to 46.06 nA. This improvement can be attributed to the desorption of adsorbates, and improvement in the inter GNR junctions. Subsequent annealing in Ar/H_2 improved the average I_{on} from 46.06 nA to 832.57 nA. The significant improvement in conductivity after annealing in Ar/H_2 might be caused by the removal of photoresist residues and other contaminants introduced during the processing steps [28]. Considering that the GNRs are dissolved in CSA, it must be noted that minor functionalization cannot be ignored. The Ar/H_2 annealing might also help to restore the structure of the GNRs, which would improve the conductivity.

While the conductivity of the GNRs improved with each annealing procedure, the On/Off ratios decreased. The largest On/Off ratio (before annealing) was ~19 and the average On/Off ratio decreased from 8.97 to 4.21 and finally to 3.04 after the Ar/H_2 annealing. Referring to figure 39 (c), this occurred due to a significant increase in the off currents.

3.4 Discussion

In the work described in this chapter, we fabricated and characterized transistors from thin films of atomically precise GNRs. While the electronic properties of these GNR based devices are very poor, they are not surprising considering the magnitude of inter-GNR junctions, domain structure of the films and other defects. However, it must be noted that the characteristics of our GNR devices are comparable to and even better than those reported in other studies of solution synthesized atomically precise GNRs [15-18]. This is because of the high structural quality and uniformity of the self-assembled GNR films.

Future work should focus on the miniaturization of the GNR devices in order to reveal the true potential of the atomically precise GNRs.

3.5 References

[1] S. S. Datta, D. R. Strachan, S. M. Khamis, and A. T. C. Johnson, "Crystallographic etching of few-layer Graphene," *Nano Letters*, vol. 8, no. 7, pp. 1912–1915, Jun. 2008.

[2] J. Campos-Delgado et al., "Bulk production of a new form of sp 2 carbon: Crystalline graphene nanoribbons — Arizona state university," *Nano Letters*, vol. 8, no. 9, pp. 2773–2778, Sep. 2008.

[3] X. Yang, X. Dou, A. Rouhanipour, L. Zhi, H. J. Räder, and K. Müllen, "Two-dimensional graphene nanoribbons," *Journal of the American Chemical Society*, vol. 130, no. 13, pp. 4216–4217, Mar. 2008.

[4] X. Li, X. Wang, L. Zhang, S. Lee, and H. Dai, "Chemically derived, ultrasmooth graphene nanoribbon semiconductors," *Science*, vol. 319, no. 5867, pp. 1229–1232, Feb. 2008.

[5] Z. Chen, Y.-M. Lin, M. J. Rooks, and P. Avouris, "Graphene nano-ribbon electronics," *Physica E*, vol. 40, no. 2, pp. 228–232, Jun. 2007.

[6] M. Y. Han, B. Özyilmaz, Y. Zhang, and P. Kim, "Energy band-gap engineering of graphene nanoribbons," *Physical Review Letters*, vol. 98, no. 20, p. 206805, May 2007.

[7] L. Jiao, L. Zhang, X. Wang, G. Diankov, and H. Dai, "Narrow graphene nanoribbons from carbon nanotubes," *Nature*, vol. 458, no. 7240, pp. 877–880, Apr. 2009.

[8] D. V. Kosynkin et al., "Longitudinal unzipping of carbon nanotubes to form graphene nanoribbons," *Nature*, vol. 458, no. 7240, pp. 872–876, Apr. 2009.

[9] A. L. Elías et al., "Longitudinal cutting of pure and doped carbon nanotubes to form graphitic nanoribbons using metal clusters as nanoscalpels," *Nano Letters*, vol. 10, no. 2, pp. 366–372, Aug. 2009

[10] L. Jiao, X. Wang, G. Diankov, H. Wang, and H. Dai, "Facile synthesis of high-quality graphene nanoribbons," *Nature Nanotechnology*, vol. 5, no. 5, pp. 321–325, Apr. 2010.

[11] J. Cai et al., "Atomically precise bottom-up fabrication of graphene nanoribbons," *Nature*, vol. 466, no. 7305, pp. 470–473, Jul. 2010.

[12] L. Talirz, P. Ruffieux, and R. Fasel, "On-surface synthesis of atomically precise graphene nanoribbons," *Advanced Materials*, vol. 28, no. 29, pp. 6222–6231, Feb. 2016.

[13] A. Narita et al., "New advances in nanographene chemistry," *Chemical Society Reviews*, vol. 44, no. 18, pp. 6616–6643, Jul. 2015.

[14] A. Narita, X. Feng, and K. Müllen, "Bottom-up synthesis of chemically precise graphene nanoribbons," *The Chemical Record*, vol. 15, no. 1, pp. 295–309, Nov. 2014.

[15] A. N. Abbas et al., "Deposition, characterization, and thin-film-based chemical sensing of ultra-long chemically synthesized graphene nanoribbons," *Journal of the American Chemical Society*, vol. 136, no. 21, pp. 7555–7558, May 2014.

[16] K. T. Kim, J. W. Lee, and W. H. Jo, "Charge-transport tuning of Solution-Processable Graphene Nanoribbons by Substitutional Nitrogen Doping," *Macromolecular Chemistry and Physics*, vol. 214, no. 23, pp. 2768–2773, Sep. 2013.

[17] R. Konnerth et al., "Tuning the deposition of molecular graphene nanoribbons by surface functionalization," *Nanoscale*, vol. 7, no. 30, pp. 12807–12811, May 2015.

[18] U. Zschieschang et al., "Electrical characteristics of field-effect transistors based on chemically synthesized Graphene Nanoribbons," *Advanced Electronic Materials*, vol. 1, no. 3, p. 1400010, Feb. 2015.

[19] A. Narita, "Synthesis of structurally well-defined and liquid-phase-processable graphene nanoribbons," *Nature Chemistry*, vol. 6, no. 2, pp. 126–132, Dec. 2013.

[20] M. G. Schwab et al., "Structurally defined graphene nanoribbons with high lateral extension," *Journal of the American Chemical Society*, vol. 134, no. 44, pp. 18169–18172, Oct. 2012.

[21] M. Cai, D. Thorpe, D. H. Adamson, and H. C. Schniepp, "Methods of graphite exfoliation," *Journal of Materials Chemistry*, vol. 22, no. 48, pp. 24992–25002, Sep. 2012.

[22] T. H. Vo et al., "Large-scale solution synthesis of narrow graphene nanoribbons," *Nature Communications*, vol. 5, p. 3189, Feb. 2014.

[23] T. Yamamoto et al., "Preparation of π-conjugated poly(thiophene-2, 5-diyl), poly(p-phenylene), and related polymers using zerovalent nickel complexes. Linear structure and properties of the π-conjugated polymers," *Macromolecules*, vol. 25, no. 4, pp. 1214–1223, Feb. 1992.

[24] C. D. Simpson et al., "Nanosized molecular propellers by cyclodehydrogenation of polyphenylene dendrimers," *Journal of the American Chemical Society*, vol. 126, no. 10, pp. 3139–3147, Feb. 2004.

[25] U. Kumar and T. X. Neenan, "Diels-alder polymerization between bis(cyclopentadienones) and acetylenes. A versatile route to new highly aromatic polymers," *Macromolecules*, vol. 28, no. 1, pp. 124–130, Jan. 1995.

[26] A. Centrone et al., "Structure of new carbonaceous materials: The role of vibrational spectroscopy," *Carbon*, vol. 43, no. 8, pp. 1593–1609, Mar. 2005.

[27] A. C. Ferrari et al., "Raman spectrum of graphene and graphene layers," *Physical Review Letters*, vol. 97, no. 18, p. 187401, Oct. 2006.

[28] M. Ishigami, J. H. Chen, W. G. Cullen, M. S. Fuhrer, and E. D. Williams, "Atomic structure of graphene on SiO_2," *Nano Letters*, vol. 7, no. 6, pp. 1643–1648, May 2007.

4. Conclusions

4.1 Summary and Future Work

In this thesis, we explored the electronics applications of carbon based materials: carbon nanotubes and graphene nanoribbons. Our work touched upon the applications of carbon nanotubes to composite fiber structures and we attempted the nanosoldering technique to improve the electrical and thermal properties of these fibers. While the nanosoldering technique showed tremendous improvement in the electrical properties, the thermal properties essentially deteriorated. We attribute this deterioration to the presence of the poly-vinyl alcohol which acts as an insulator and could be inhibiting the true potential of the nanosoldering technique. Future work on this project will focus on creating pure CNT fibers and applying the nanosoldering technique accordingly. When the metal molecules were used, we could view them and verify their presence at the junctions using SEM and XPS. Unfortunately, the carbon based structures that result from the thermal decomposition of the precursor cannot been seen in SEM. In order to verify the presence of these structures at the junctions, we believe that aberration corrected TEM could provide high-resolution imaging and should be used.

In addition, we also fabricated and characterized transistors from thin films of graphene nanoribbons. While the electronic properties of these transistors were poor, the interfacial self-assembly approach used for the fabrication of the thin films allowed for a streamlined process to fabricate and characterize multiple transistors. We attribute the poor performance to the possible intercalation of the CSA, and the numerous inter-GNR junctions. Future work on this project should involve reducing device channel lengths and optimizing the device structure. Alternatively, a different type of GNR that exhibits better electronic properties could be used for the channel material.

As mentioned in the introduction, carbon's material abundance makes it compelling for use as a building block in technology. While there are challenges associated with the processing of the various nanoscale allotropes of carbon, their superb electrical, thermal and chemical properties could address the issues associated with the materials that form the backbone of modern electronics. Future work centered on the processing issues of the nanoscale allotropes of carbon could solve the prevalent problems faced by current materials and help build better electronics for a better world.